An Introduction to Relativistic Hydrodynamics Simulation and Its Application

Jeongbhin Seo(UNIST)

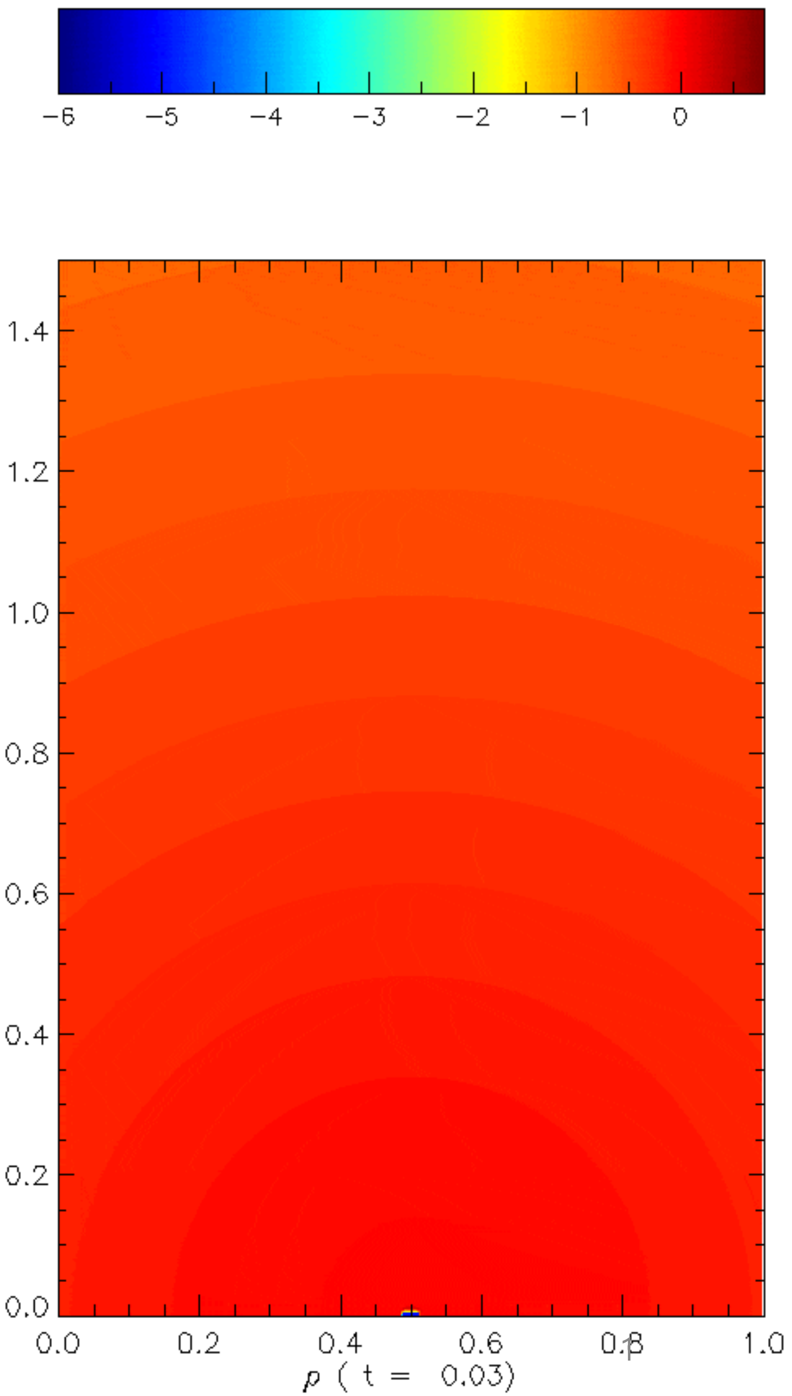

부산대학교
PUSAN NATIONAL UNIVERSITY

A New Code for Relativistic Hydrodynamic simulation

Summary of Newly developed RHD code

To simulate **accurate** and **realistic** relativistic flow, we adopt the following schemes

1. **5^{th} order accurate WENO scheme (Jiang & Shu 1996, Jiang & Wu 1999)** for spatial integration

2. **Strong stability preserving Runge-Kutta (SSPRK) scheme (Spiteri & Ruuth 2002)** for time integration

3. **Realistic equation of state (RC, Ryu et al 2006)** to treat the flow with γ=4/3 - 5/3

4. **Transverse-flux averaging** for multi-dimensional flows **(Buchmüller et al. 2016)**

5. **Modification of eigenvalues for Suppression of Carbuncle Instability (Fleischmann et al. 2020)**

RHD equations

$$\frac{\partial D}{\partial t} + \frac{\partial}{\partial x_j}(D v_j) = 0$$

$$\frac{\partial M_i}{\partial t} + \frac{\partial}{\partial x_j}(M_i v_j + p\delta_{ij}) = 0$$

$$\frac{\partial E}{\partial t} + \frac{\partial}{\partial x_j}[(E + p)v_j] = 0$$

(1) Mass conservation
(2) Momentum conservation
(3) Energy conservation

$D = \rho\Gamma$: mass density
$M_i = \Gamma^2 h\rho v_i$: momentum density
$E = \Gamma^2 h\rho - p$: energy density

ρ : proper rest mass density Γ: Lorentz factor h : specific enthalpy
v_i : fluid three vector p : isotropic gas pressure

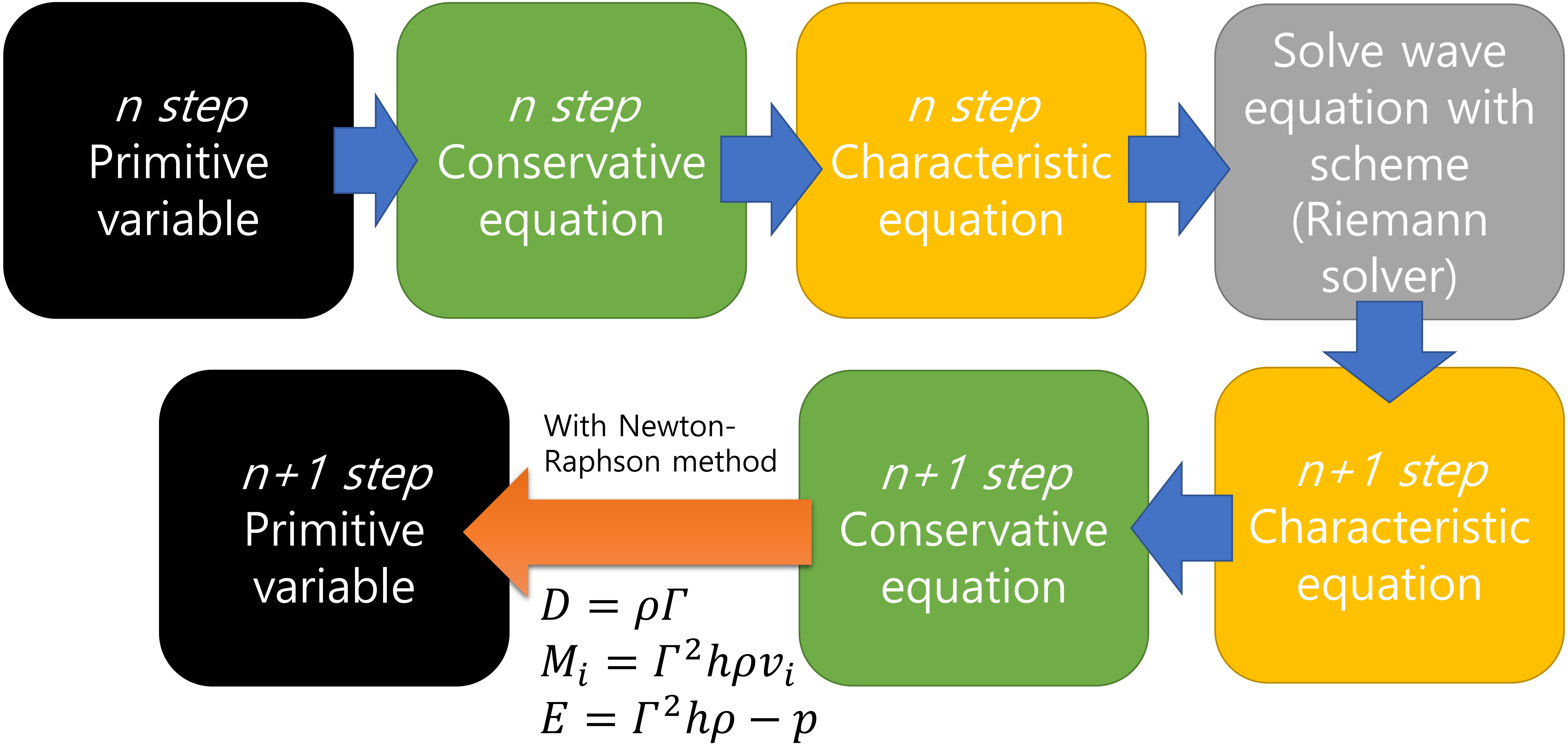
n step Primitive variable
n step Conservative equation
n step Characteristic equation
Solve wave equation with scheme (Riemann solver)
n+1 step Characteristic equation
n+1 step Conservative equation
With Newton-Raphson method
$D = \rho\Gamma$
$M_i = \Gamma^2 h\rho v_i$
$E = \Gamma^2 h\rho - p$
n+1 step Primitive variable

Equation of state (EOS)

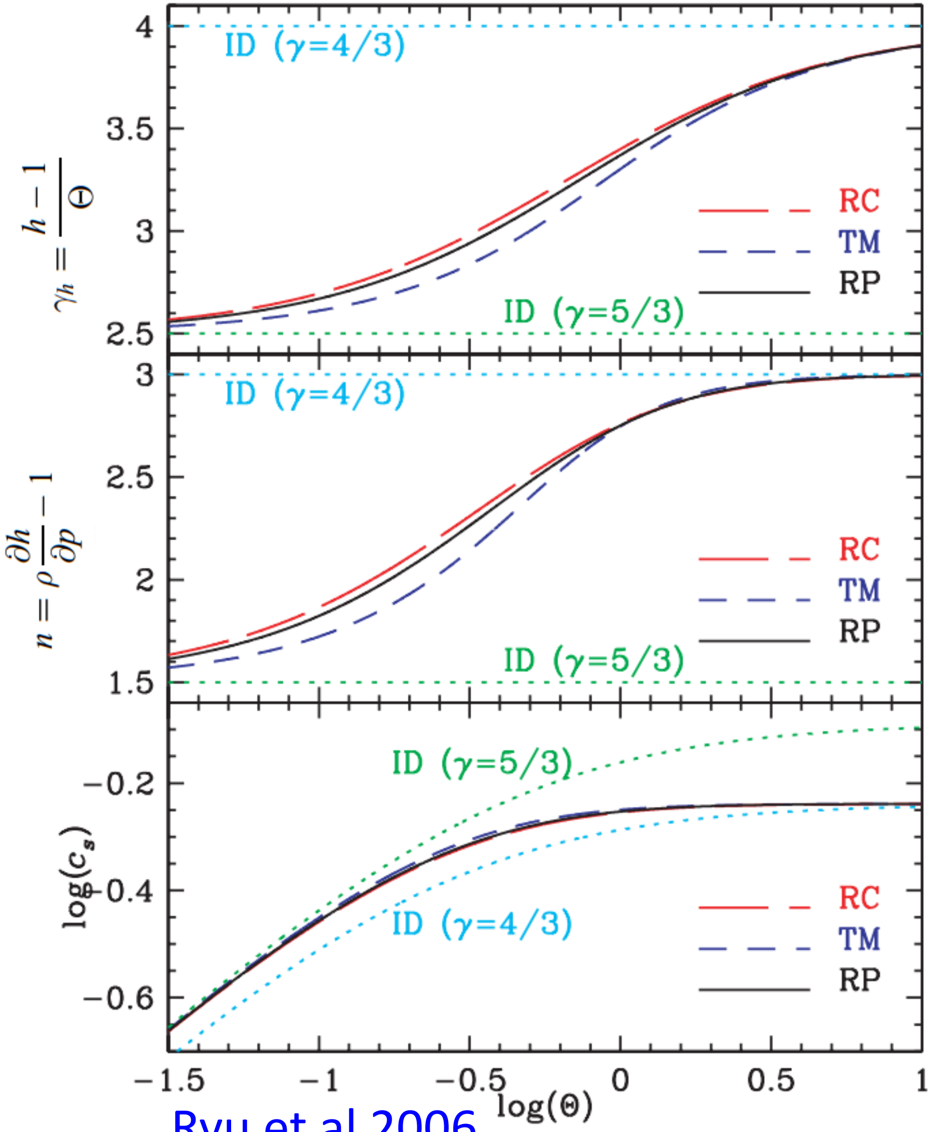

Ryu et al 2006

For relativistic flows with thermal speed of particles ~ c, the following EOSs that approximate the EOS of single-component perfect in relativistic regime (RP) is used:

RP: $$h(p,\rho) = \frac{K_3(1/\Theta)}{K_2(1/\Theta)},$$ (K's – Bessel functions)

$\Theta = p/\rho$ is a temperature-like variable.

(RP is too expensive to be implemented in numerical codes).

RC: $$h = 2\,\frac{6\Theta^2 + 4\Theta + 1}{3\Theta + 2}.$$ (Ryu et al 2006)

Weighted Essentially Non-Oscillatory (WENO) scheme

Calculating the physical flux using a **5th order accurate finite-difference (FD) WENO reconstruction.**

$$q'_{i,j,k} = q_{i,j,k} - \frac{\Delta t}{\Delta x}\left(F_{i+\frac{1}{2},j,k} - F_{i-\frac{1}{2},j,k}\right) - \frac{\Delta t}{\Delta y}\left(G_{i,j+\frac{1}{2},k} - G_{i,j-\frac{1}{2},k}\right) - \frac{\Delta t}{\Delta z}\left(H_{i,j,k+\frac{1}{2}} - H_{i,j,k-\frac{1}{2}}\right),$$

$$\begin{aligned} F_{i+\frac{1}{2}} &= \frac{1}{12}\left(-F_{i-1} + 7F_i + 7F_{i+1} - F_{i+2}\right) \\ &+ \sum_{s=1}^{5}\Big[-\varphi_N\left(\Delta F^{s+}_{i-\frac{3}{2}}, \Delta F^{s+}_{i-\frac{1}{2}}, \Delta F^{s+}_{i+\frac{1}{2}}, \Delta F^{s+}_{i+\frac{3}{2}}\right) \\ &+ \varphi_N\left(\Delta F^{s-}_{i+\frac{5}{2}}, \Delta F^{s-}_{i+\frac{3}{2}}, \Delta F^{s-}_{i+\frac{1}{2}}, \Delta F^{s-}_{i-\frac{1}{2}}\right)\Big] R^s_{i+\frac{1}{2}}, \end{aligned}$$

$$\varphi_N(a,b,c,d) = \frac{1}{3}\omega_0(a - 2b + c) + \frac{1}{6}\left(\omega_2 - \frac{1}{2}\right)(b - 2c + d).$$

$$\omega_0 = \frac{\delta_0}{\delta_0 + \delta_1 + \delta_2}, \quad \omega_2 = \frac{\delta_2}{\delta_0 + \delta_1 + \delta_2}.$$

Tests for three different WENO weight functions,

1. WENO JS (Jiang & Shu 1996),
2. WENO Z (Borges et al. 2008),
3. WENO ZA (Liu et al. 2018).

WENO-Z is both **accurate** and **robust.**

→ **Selected as the default scheme**

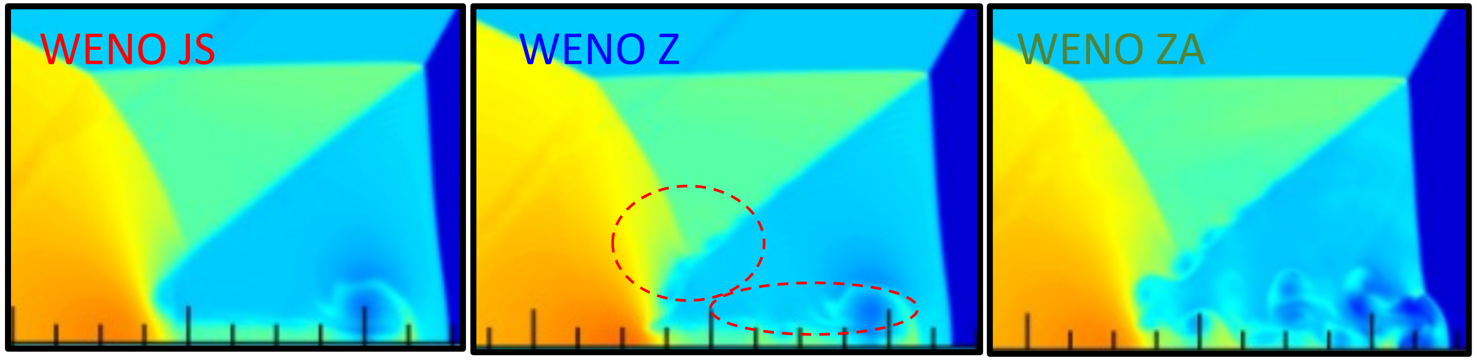

Relativistic double-Mach reflection problem with an inclined shock

$$\delta_r^{JS} = \frac{C_r}{(\epsilon + IS_r)^2}, \quad r = 0,1,2, \qquad \text{WENO JS}$$

$$\delta_r^{Z} = C_r\left(1 + \left(\frac{\tau_5}{\epsilon + IS_r}\right)^2\right), \quad r = 0,1,2, \qquad \text{WENO Z}$$

$$\delta_r^{ZA} = C_r\left(1 + \frac{A \cdot \tau_6}{\epsilon + IS_r}\right), \quad r = 0,1,2, \qquad \text{WENO ZA}$$

Strong stability preserving Runge–Kutta (SSPRK)

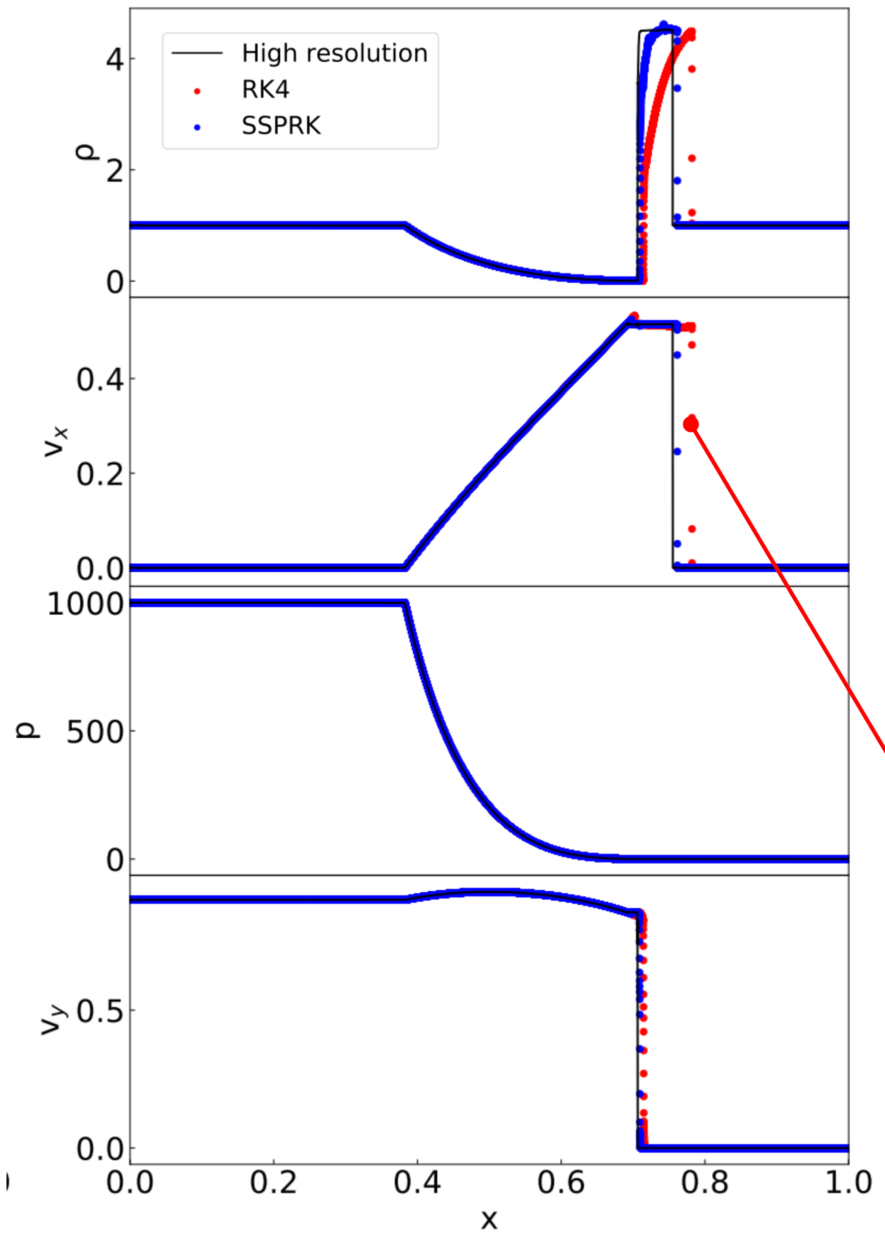

(Spiteri & Ruuth 2002)

$$\boldsymbol{q}^{(0)} = \boldsymbol{q}^n, \qquad \boldsymbol{q}^{(l)} = \sum_{m=0}^{l-1} \left(\chi_{lm}\boldsymbol{q}^{(m)} + \Delta t \beta_{lm} \boldsymbol{\mathcal{L}}^{(m)}\right), \quad l = 1, 2, \cdots, 5, \qquad \boldsymbol{q}^{n+1} = \boldsymbol{q}^{(5)}.$$

$\rho = 1$ $v_x = 0$ $v_y = 0.9c$ $p = 10^3$	$\rho = 1$ $v_x = 0$ $v_y = 0$ $p = 10^{-2}$

Initial condition of this shock tube test

- **Most of the code with WENO uses 4th order Runge-Kutta (RK4) scheme for time integration.**
- **In RHD simulation, shock with transverse flow is hard to simulate.**
- **In such cases, even shock positions cannot be followed properly. It is a well-known problem in RHD simulations.**
- **With the SSPRK method, the code can simulate harsh conditions with strong stability.**

Treatment for multi-dimensional problems

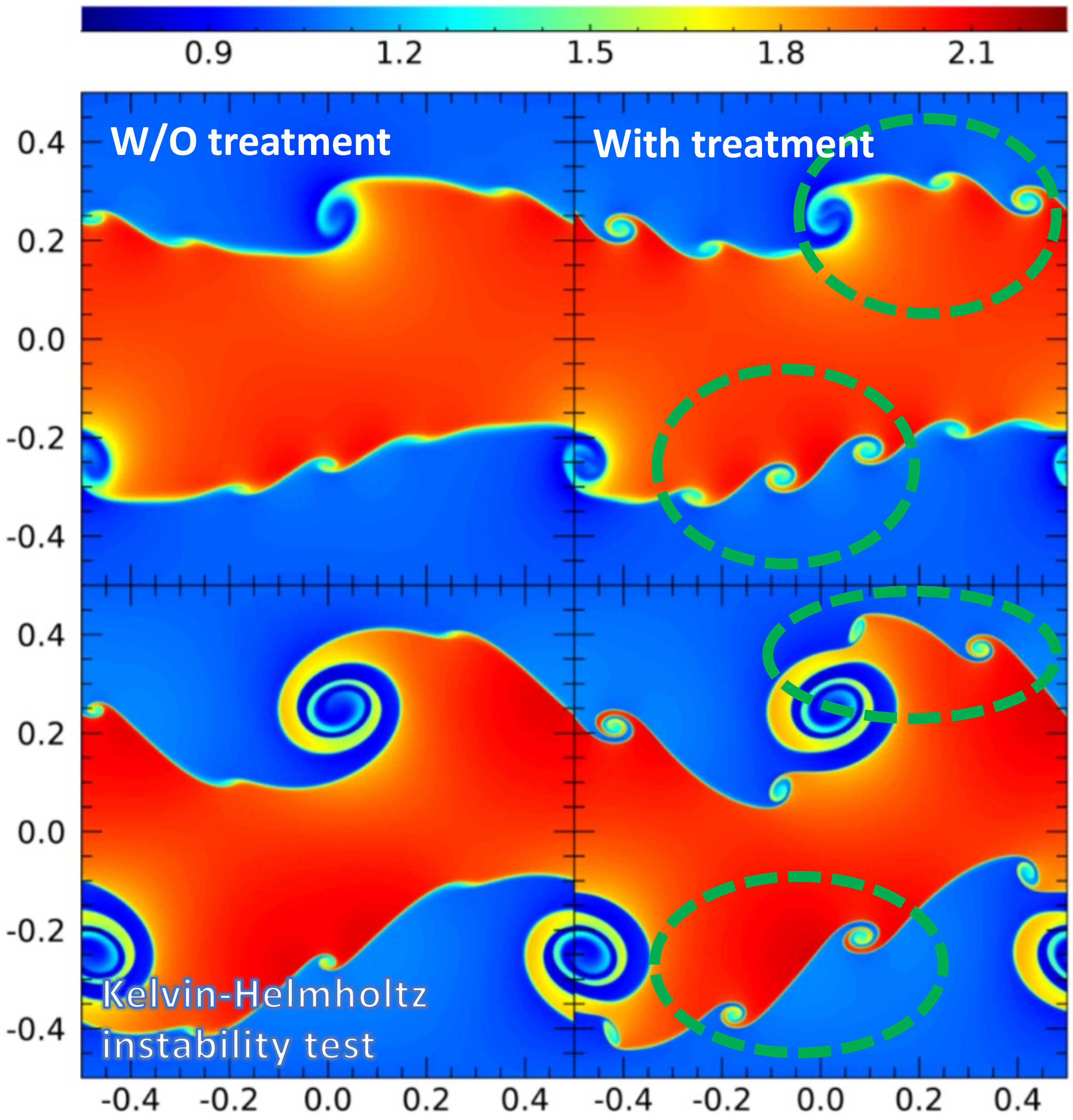

$$\bar{q}_{i,j,k} = q_{i,j,k} - \frac{1}{24}\left(q_{i,j-1,k} - 2q_{i,j,k} + q_{i,j+1,k}\right) - \frac{1}{24}\left(q_{i,j,k-1} - 2q_{i,j,k} + q_{i,j,k+1}\right),$$

$$\bar{F}_{i\pm\frac{1}{2},j,k} = F_{i\pm\frac{1}{2},j,k} + \frac{1}{24}\left(F_{i\pm\frac{1}{2},j-1,k} - 2F_{i\pm\frac{1}{2},j,k} + F_{i\pm\frac{1}{2},j+1,k}\right) + \frac{1}{24}\left(F_{i\pm\frac{1}{2},j,k-1} - 2F_{i\pm\frac{1}{2},j,k} + F_{i\pm\frac{1}{2},j,k+1}\right).$$

- **Transverse flux averaging scheme is proposed as a modified dimension-by-dimension method for FV WENO schemes, which leads to high order accuracies for smooth solutions** (Buchmüller et al. 2016)**.**

- **By bringing this scheme to our FD WENO scheme, we improve the accuracies for multi-dimensional flows.**

Treatment for carbuncle instability

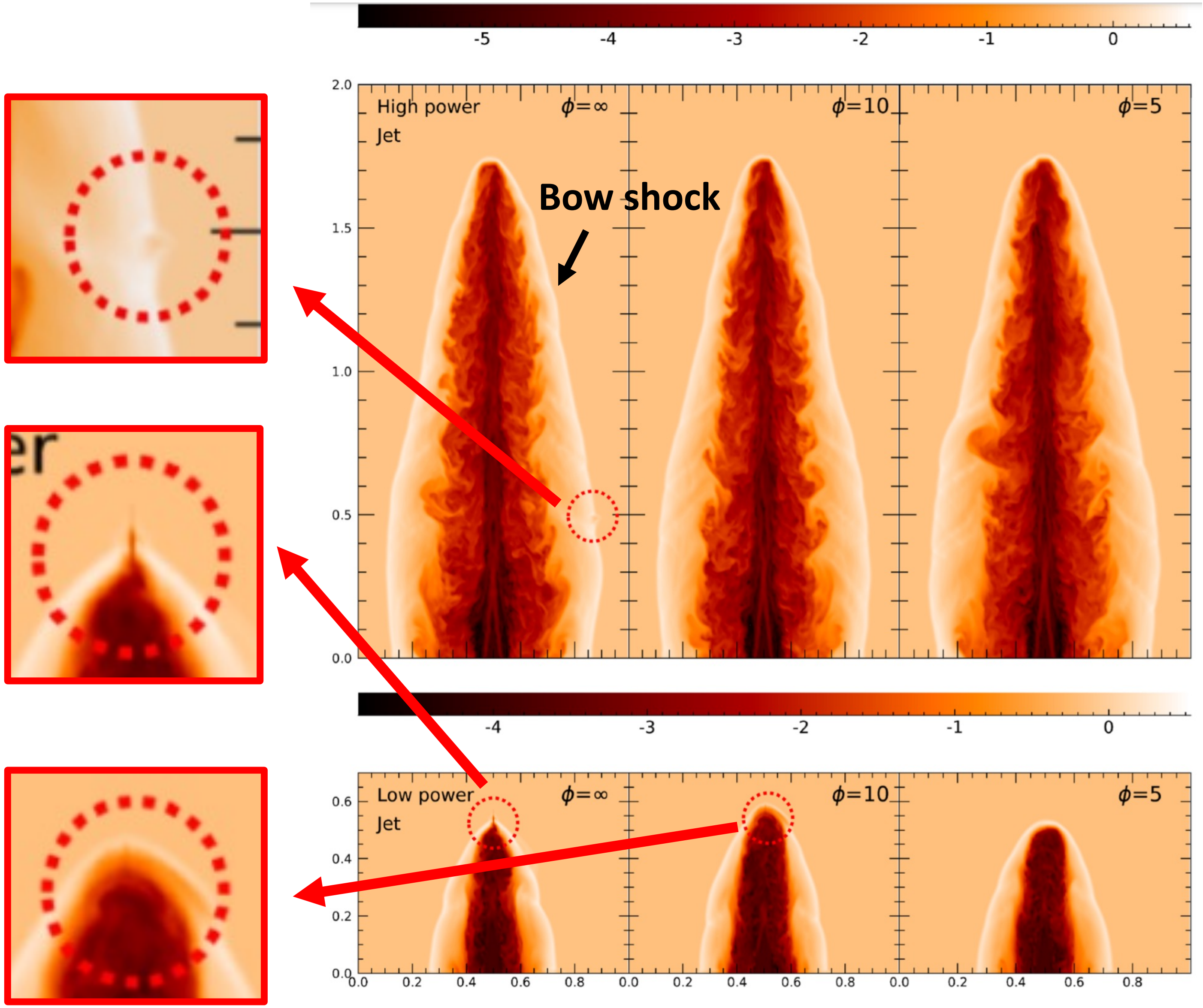

Unphysical structures due to carbuncle instability

- **Carbuncle instability arises at slow-moving grid-aligned shocks, e.g., bow shock of the jet.**

- **modified eigenvalues for RHD**

$$c'_s = \min(\phi|v_x|, c_s),$$

(Fleischmann et al. 2020)

$$\lambda'_{1,5} = \frac{(1 - c'^2_s)v_x \mp c'_s/\Gamma\sqrt{\mathcal{Q}}}{1 - c'^2_s v^2},$$

$$\lambda'_{2,3,4} = v_x,$$

$$\mathcal{Q} = 1 - v_x^2 - c'^2_s(v_y^2 + v_z^2)$$

ϕ is a tunable parameter

➔ This can effectively suppress Carbuncle instability

Application to astrophysical jets

Application to astrophysical jets

Our state-of-art RHD code can simulate accurate and realistic

Realistic EOS + 5th order WENO + SSPRK

+ Transverse-flux averaging + Modification of eigenvalues

By using the
high-resolution capability

- **Follow detailed non-linear structures, e.g., shock, shear, and turbulence, generated in the jet-induced flow**
- **Analyze characteristics of these structures**
- **Study particle acceleration by these structures**

What are Ultra-high energy cosmic rays (UHECRs)?

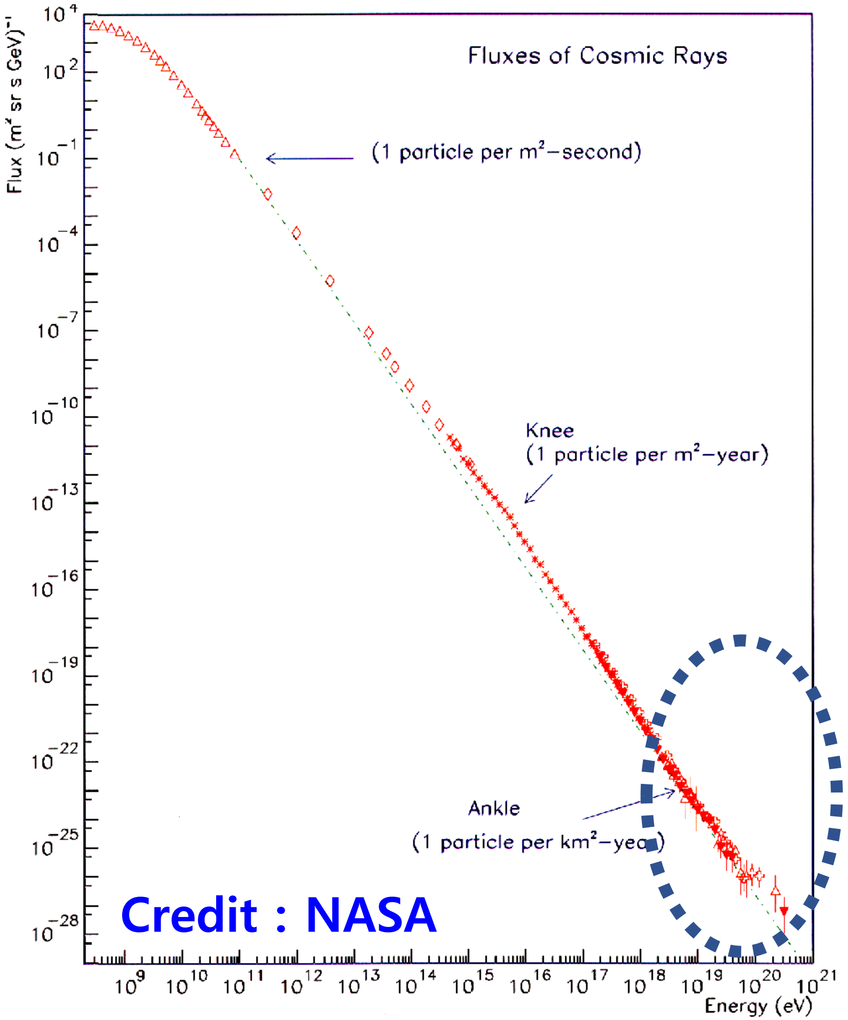

Cosmic ray energy spectrum

UHECR
$\geq 10^{18}$eV(EeV)

Hillas Energy

$$E_{max} = 0.9\text{EeV}\, Z_i \left(\frac{B}{\mu\text{G}}\right)\left(\frac{v_s}{c}\right)\left(\frac{r}{\text{kpc}}\right)$$

$v_s \sim c, r_s \sim \text{kpc}$, and $B \sim \mu\text{G}$

for shock generated in jet-induced flows of Radio galaxy jet

→ Radio galaxy jet is a good candidate for generating UHECRs

Seo et al 2021

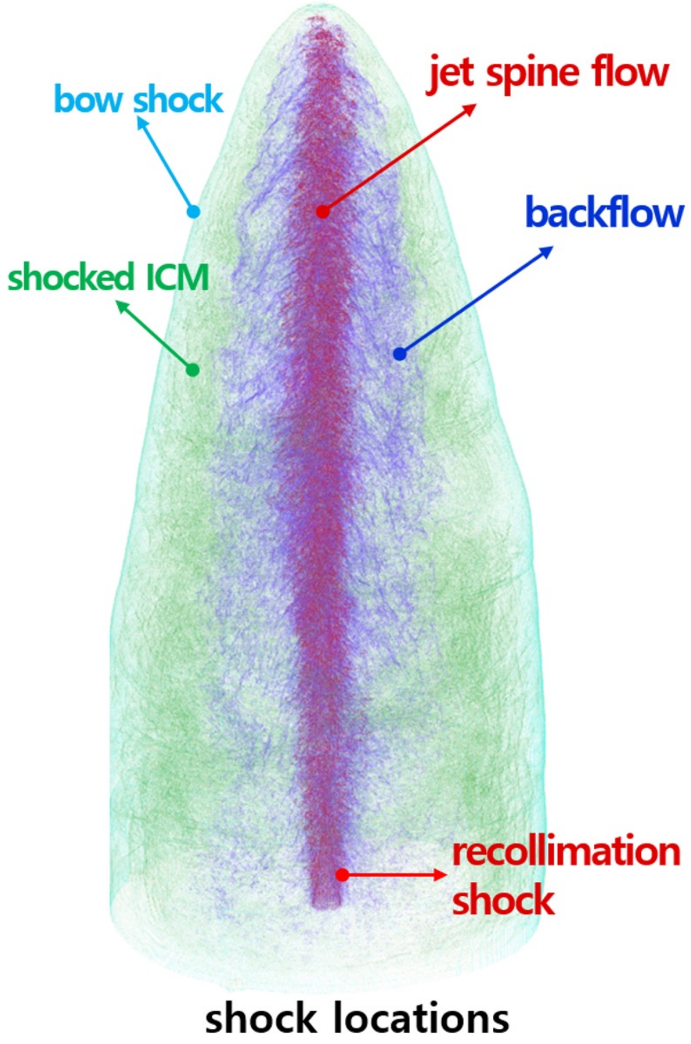

Shock distribution in jet-induced flows of FRII galaxy

Aim of this study

- Radio galaxy : relativistic jet that emits radio synchrotron emission

- Relativistic jets : Promising candidates of the UHECRs generator (Blandford et al. 2019; Rieger 2019; Hardcastle & Croston 2020; Matthews et al. 2020)

- classified into two Fanaroff-Riley (FR) types.
  FR-I : Mildly relativistic flume like jet, brightest center
  FR-II : Relativistic jet, brightest edge (Hot spot), radio lobe (cocoon)

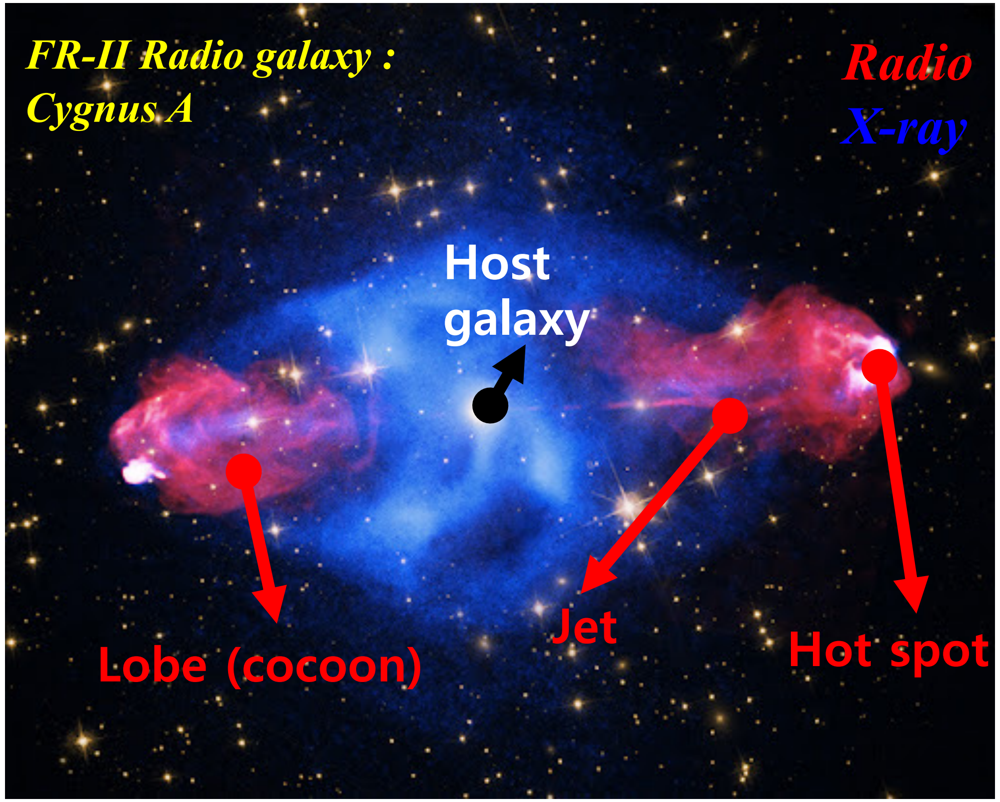

X-ray: NASA/CXC/SAO; Optical: NASA/STScI; Radio: NSF/NRAO/AUI/VLA

- Main question:

Can FR-II radio galaxies generate UHECRs?

Previous study of the UHECRs acceleration in Radio galaxy jet

Matthews et al 2019

- **Diffusive shock acceleration**
- Performed **RHD** simulation (PLUTO code)
- **Hillas energy** of the backflow shocks is presented (~10^{19}eV for proton)
- **Figure :** Shock surface they found, within the jet (cyan), within backflow (orange)

Kimura et al 2018 &
Ostrowski et al 1998

- **Discrete shear acceleration**
- Performed **Monte-Carlo** simulations with simple cylindrical configuration
- **Energy spectrum** of accelerated particles is presented
- **Figure :** schematic picture of shear acceleration in a jet- cocoon system of an AGN.

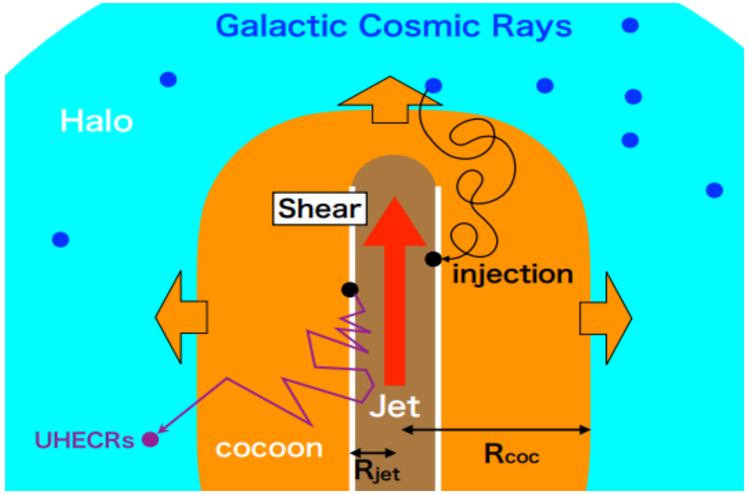

Caprioli 2018 &
Mbarek et al 2019, 2021

- **“expresso” acceleration**
- Performed **Monte-Carlo** simulations using simulated MHD jet configuration
- **Energy spectrum** of acceleration particle is presented
- **Figure :** Schematic trajectory of a galactic CR reaccelerated by a relativistic jet

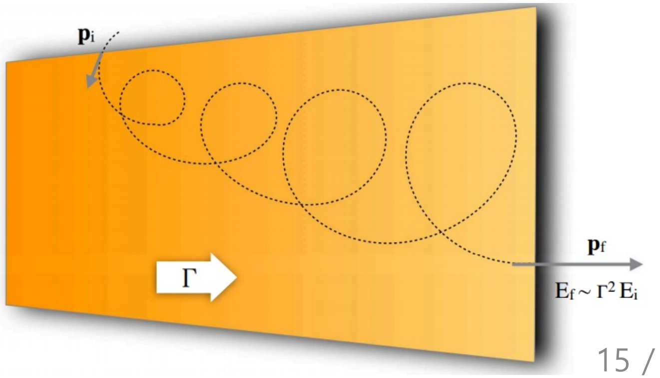

Flow chart of this study

Title of the study	Development of a new code for Relativistic Hydrodynamics (RHD)	Simulations of FR-II jets: Structures and Dynamics	Monte Carlo Simulations for CR acceleration, using simulated FR-II jets
Main topic	• Develop high order RHD code • 5th order WENO + 4th order SSPRK • Adopt Realistic equation of state • Perform various code test	• Perform RHD jet simulation • Study parameter dependency of the morphology and energetics of the jet • Analyze non-linear structures	• Develop Cosmic ray transport code • Analyze the acceleration process that occurred inside the jets • Present UHECRs spectrum accelerated through FR-II jets

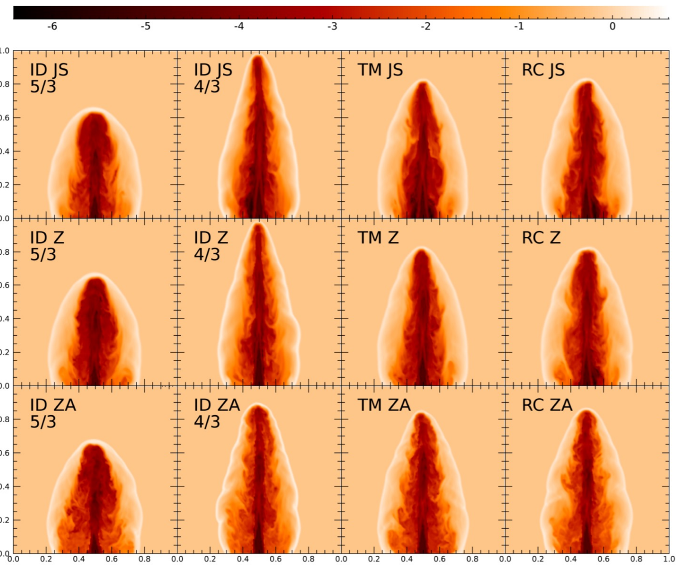

Developing Realistic and accurate RHD code

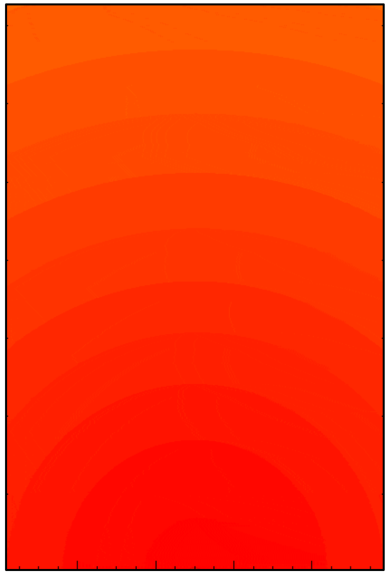

RHD jet simulation

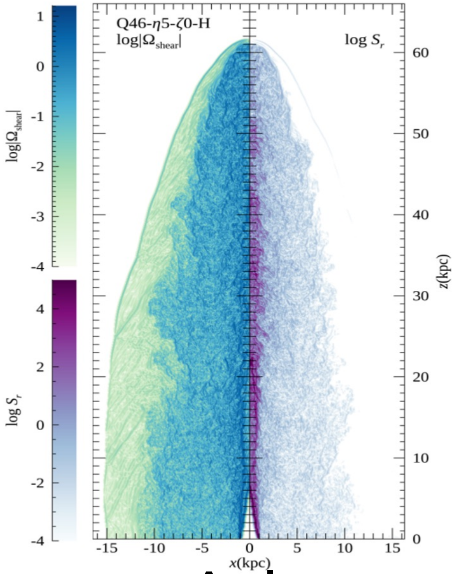

Analyze non-linear structures

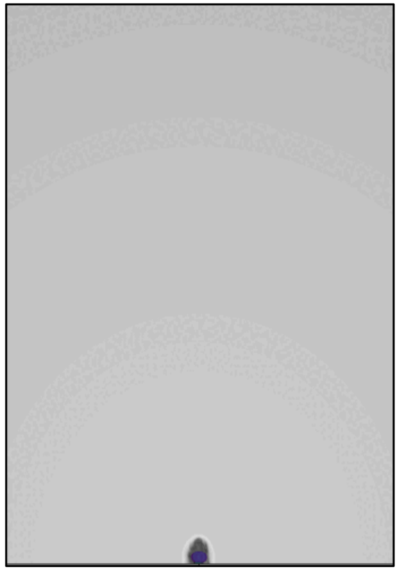

Monte-Carlo simulation

Structures generated in the jet-induced flow

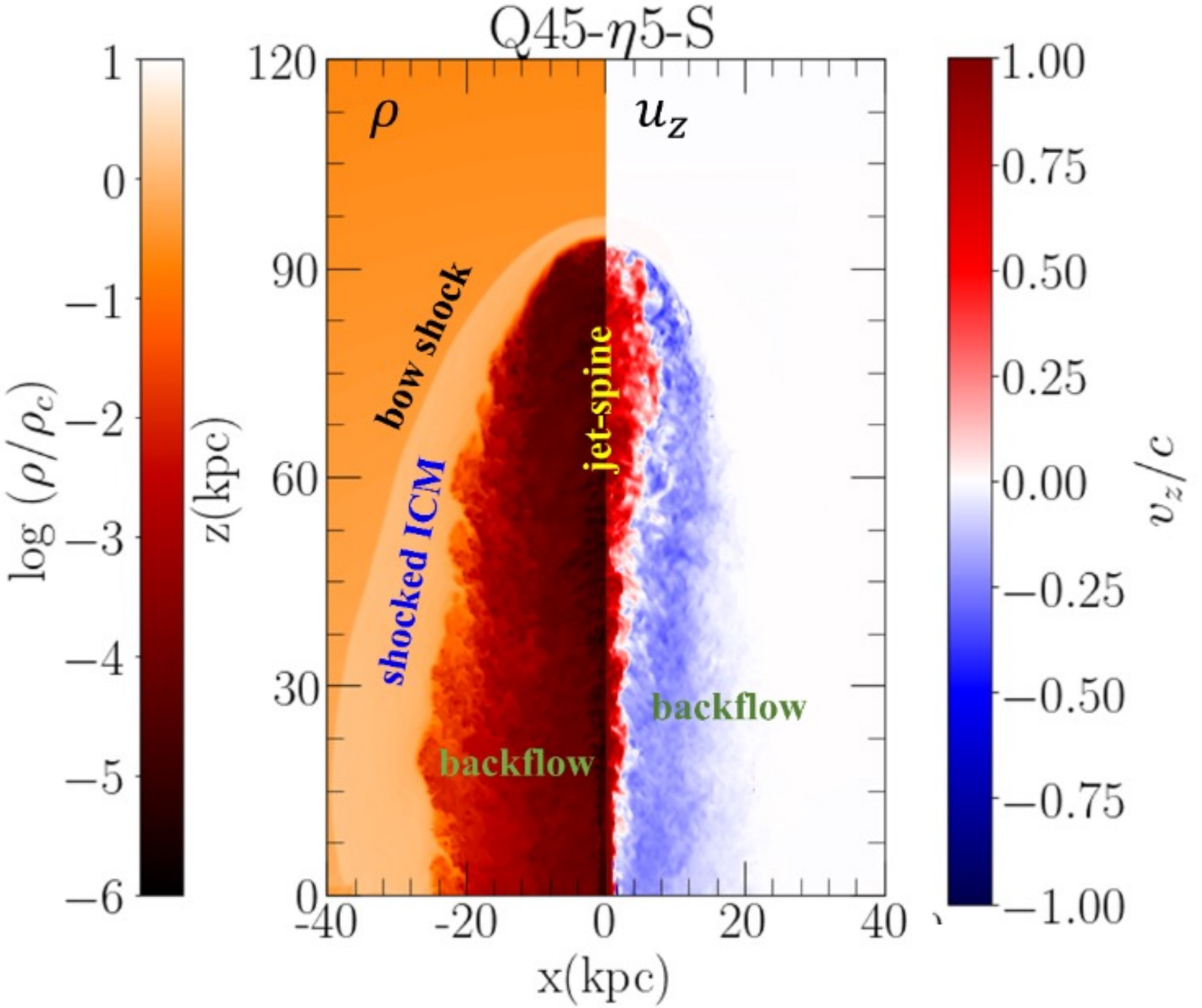

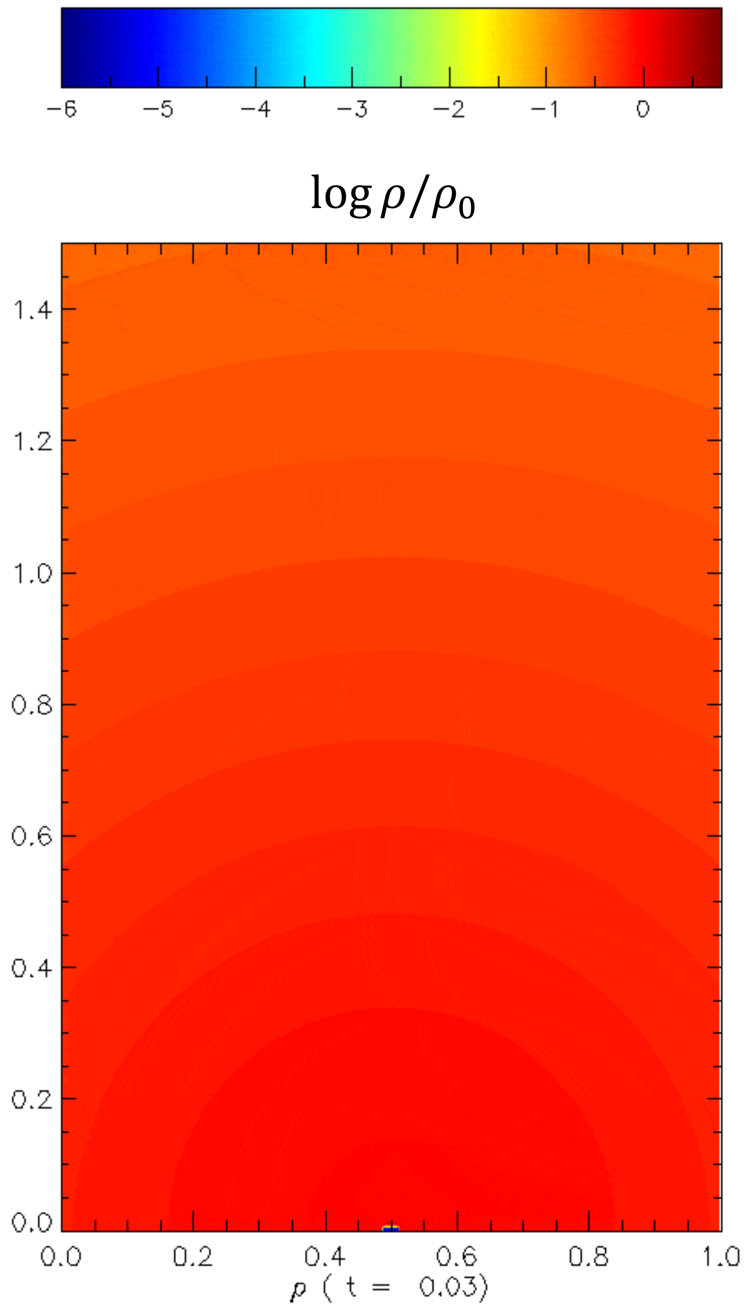

The jet is halted at the **termination shock**, while the backflow forms a **cocoon/lobe** that encompasses the **jet spine.**

Step 1. Development of a new code for Relativistic Hydrodynamics (RHD)

Step 2. Simulations of FR-II jets: Structures and Dynamics

RHD simulations of relativistic jets

Seo et al. 2021b

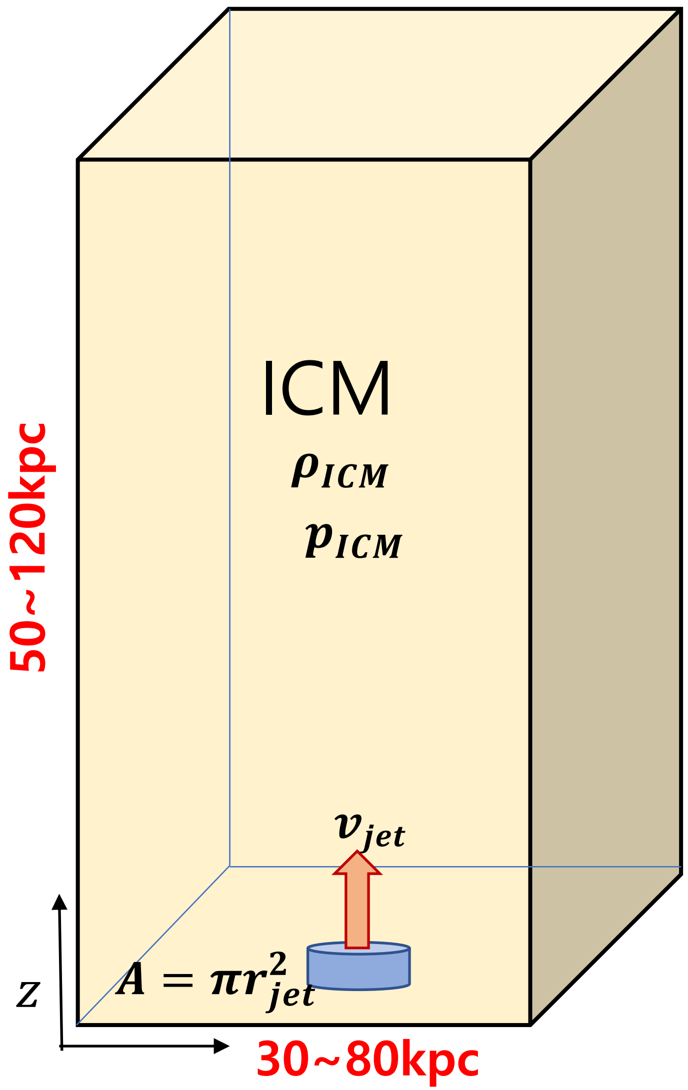

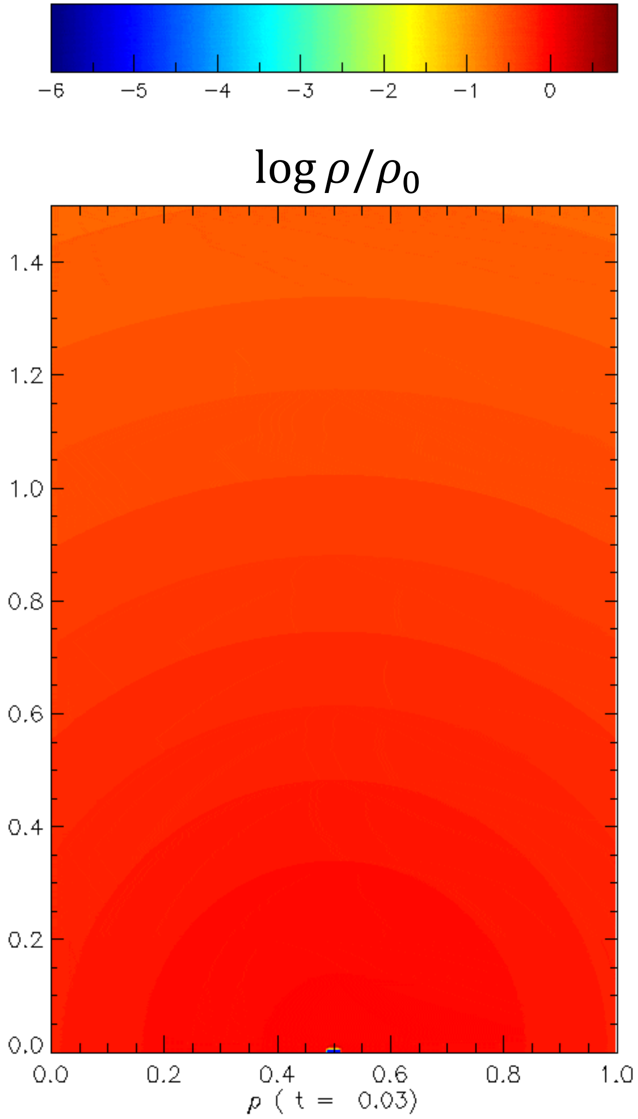

- Relativistic HD simulation (**RHD**, No $\vec{B}$ field)
- **FR-II Type radio galaxy**
- **Grid resolution:** $\Delta x \sim 0.1\text{kpc}$
- **T$_{dyn}$** $\sim \frac{100kpc}{0.1c} \sim$ **a few Myr**
- **Isothermal Cluster profile**

$$\rho(r) = \rho_0 \left[1 + \left(\frac{r}{r_c}\right)^2\right]^{-3\beta/2}$$

r : distance from the center of the cluster
r_c : core radius, 50kpc, β: 0.5

Main model parameters

Model name	Q_j (erg s^{-1})	$\eta \equiv \frac{\rho_j}{\rho_b}$	$\zeta \equiv \frac{p_j}{p_b}$	v_j/c
Q45-η5-ζ0	3.34E+45	1.E-05	1	0.9905
Q46-η5-ζ0	3.34E+46	1.E-05	1	0.9990
Q46-η5-ζ0-H				
Q47-η5-ζ0	3.34E+47	1.E-05	1	0.9999
Q47-η5-ζ0-H				
Q45-η4-ζ0	3.34E+45	1.E-04	1	0.9729
Q45-η3-ζ0	3.34E+45	1.E-03	1	0.8646
Q46-η4-ζ0	3.34E+46	1.E-04	1	0.9968
Q46-η3-ζ0	3.34E+46	1.E-03	1	0.9774
Q47-η4-ζ0	3.34E+47	1.E-04	1	0.9997
Q47-η3-ζ0	3.34E+47	1.E-03	1	0.9973
Q45-η4-ζ1	3.34E+45	1.E-04	10	0.9157
Q46-η4-ζ1	3.34E+46	1.E-04	10	0.9905
Q47-η4-ζ1	3.34E+47	1.E-04	10	0.9990

Jet power : The rate of the inflow energy through the jet inlet, excluding the mass energy

$$Q_j = \pi r_j^2 u_j \left(\Gamma_j^2 \rho_j h_j - \Gamma_j \rho_j c^2\right)$$

$\boldsymbol{r_j}$: jet radius, $\boldsymbol{u_j}$: initial jet velocity,
$\boldsymbol{\Gamma_j}$: Lorentz factor, $\boldsymbol{\rho_j}$: jet density,
$\boldsymbol{h_j}$: spicific enthalpy, $\boldsymbol{c}$: speed of light

To investigate the effect of

- **Jet power**
- **Jet density**
- **Jet pressure**

on morphology & non-linear structures

Properties of Shocks

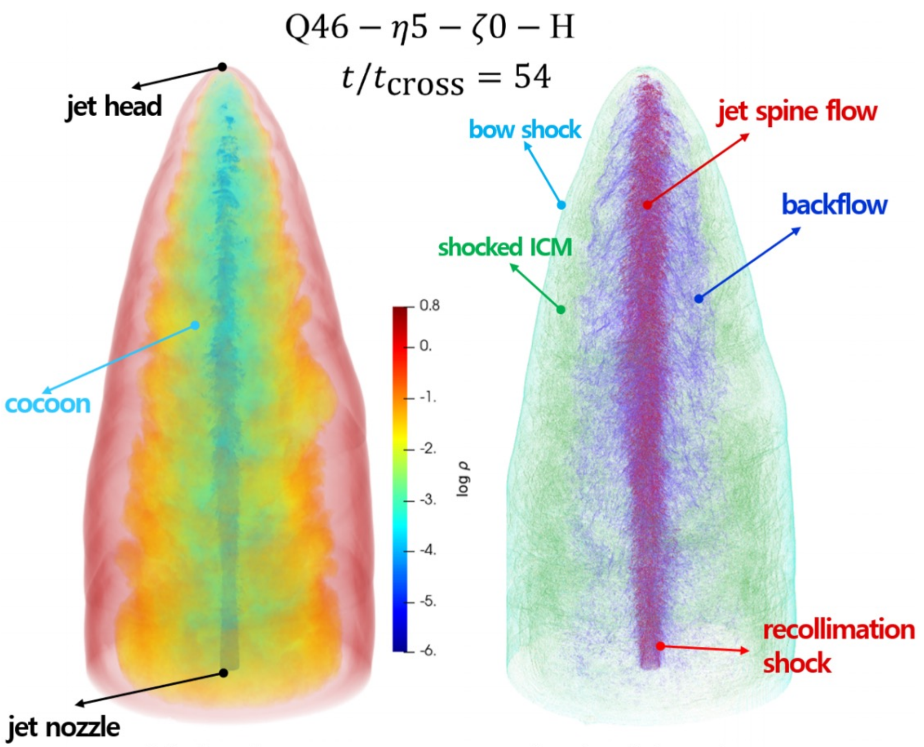

(a) density (b) shock locations

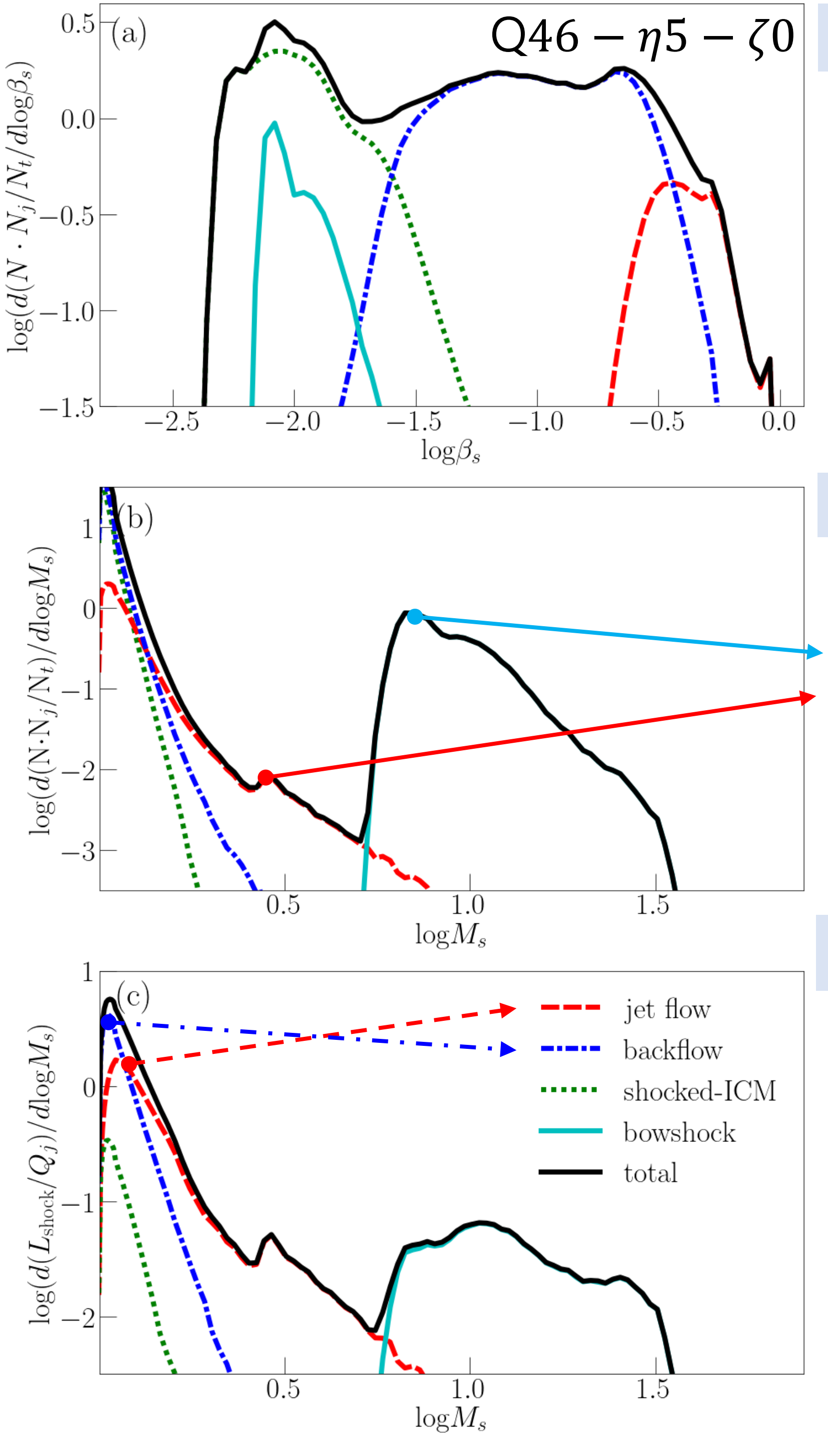

Shock speed

Range of $\beta_s = v_s/c$
(v_s: shock velocity)
jet flow : 0.2-1.0
Backflow : 0.01-0.4
Bowshock &
Shocked-ICM : < 0.005-0.05

Mach number

Peaks of $N(M_s)$ occur at
-M_s~6.5 for the bow shock
-M_s~3 for the recollimation shock
Other shocks have power-law PDF, $N(M_s) \propto {M_s}^{-5\sim-13}$

Kinetic energy dissipation rate

$$\Delta\Phi_{\rm shock} \equiv \Gamma_1(\Gamma_1 - 1)\rho_1 c^2 v_1 - \Gamma_2(\Gamma_2 - 1)\rho_2 c^2 v_2$$

$$L_{\rm shock}(M_s) = \sum_{\log M_s}^{\log M_s + d\log M_s} \Delta\Phi_{\rm shock} A_{\rm shock},$$

Shocks in jet flow & backflow have high kinetic energy dissipation rates.

Properties of Shear and Turbulence

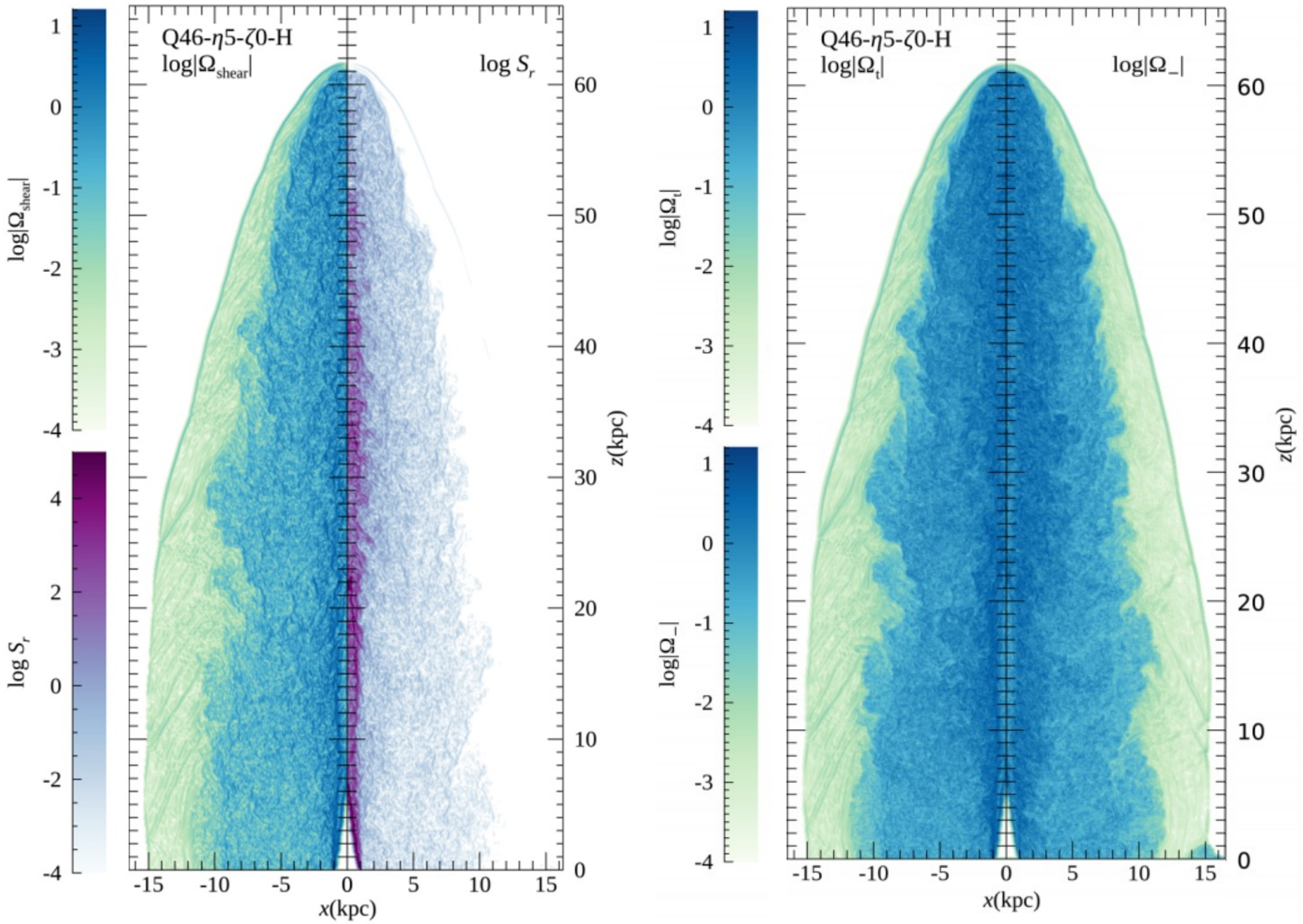

Shear

$$\Omega_{\rm shear} \equiv |\partial v_z/\partial r|$$

Relativistic shear coefficient

$$S_r = \frac{\Gamma_v^4}{15}\left(\frac{\partial v_z}{\partial r}\right)^2,$$ (Rieger 2019)

Shear is strongest at jet-cocoon boundary and inside the jet flow
S_r is largest in the jet flow.

Total vorticity

$$\boldsymbol{\Omega}_t = \boldsymbol{\nabla} \times \boldsymbol{v}$$

Vorticity excluding shear

$$\boldsymbol{\Omega}_- = \boldsymbol{\Omega}_t + \frac{\partial v_z}{\partial r}\hat{\boldsymbol{\theta}},$$

Backflow has large vorticity due to Turbulence

Shock energy dissipation rate

$$\mathcal{L}_{\text{shock}} = \int_{M_{\min}} L_{\text{shock}}(M_s)\, d\log M_s,$$

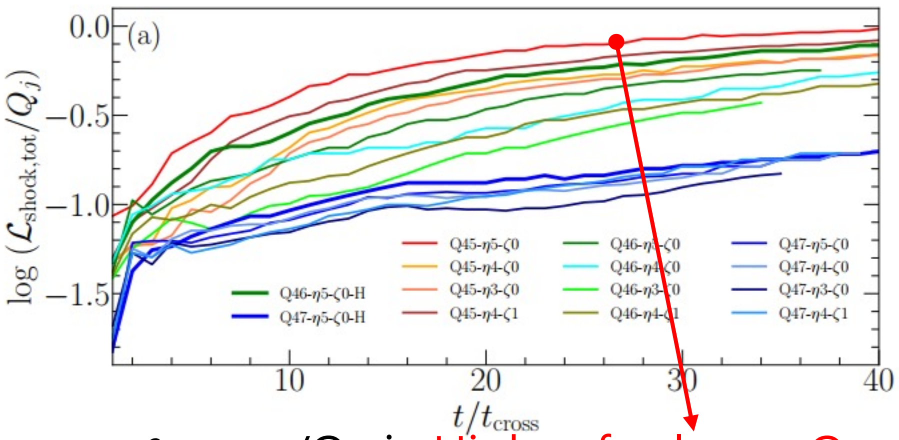

$\mathcal{L}_{\text{shock}}/Q_j$ is Higher for lower Q_j

$\mathcal{L}_{\text{shock}}/Q_j$ is Higher for lower $\dot{M}$

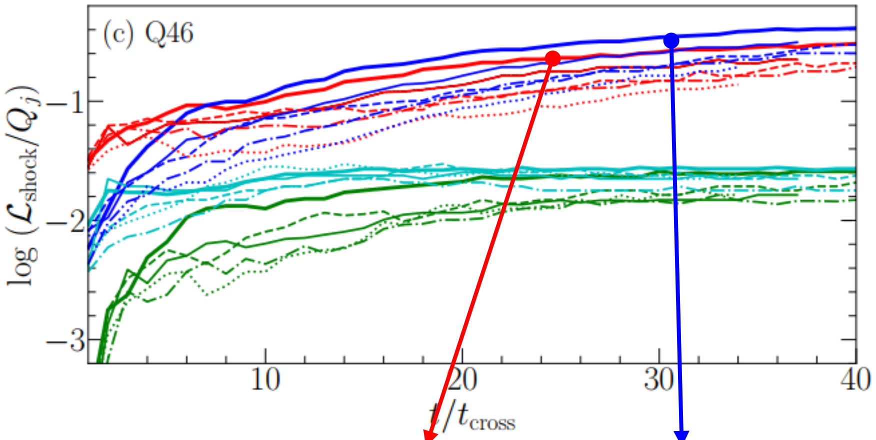

Shocks in the jet flow and backflow are most important in energy dissipation

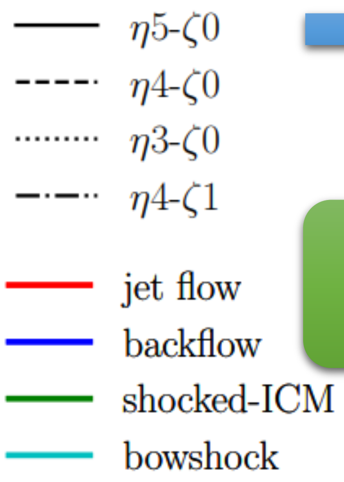

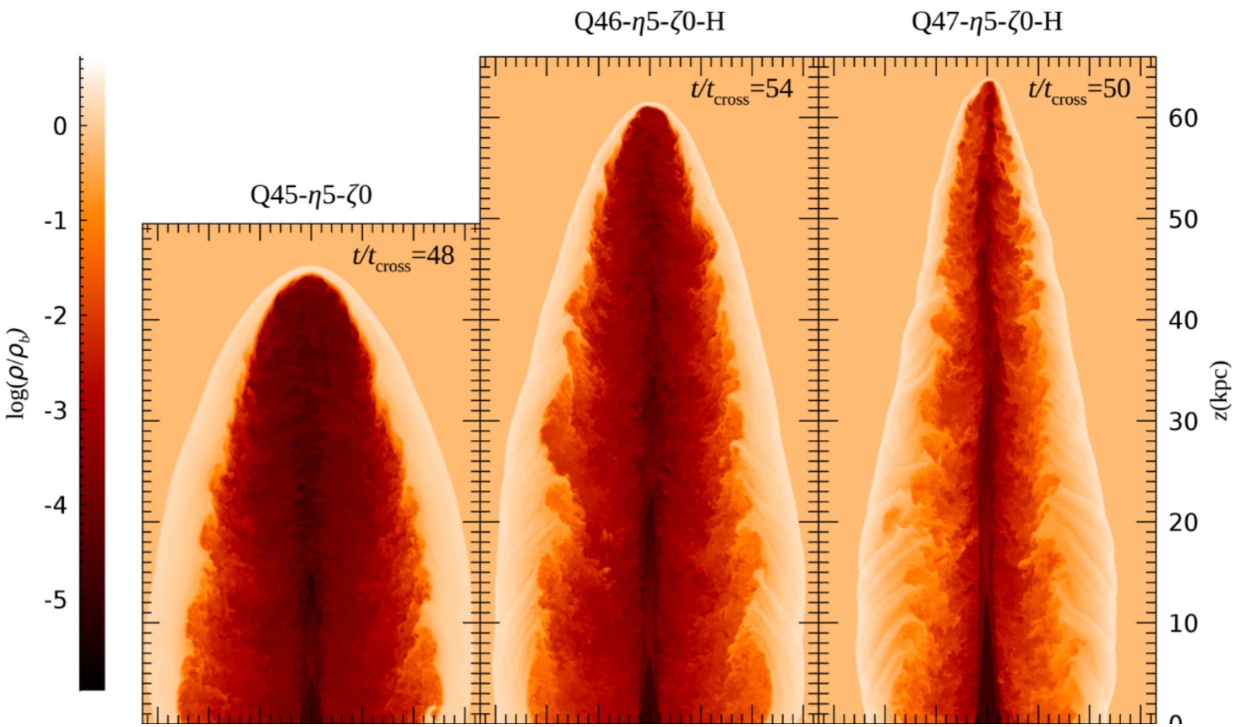

Higher Q_j, Lower $\mathcal{L}_{\text{turb}}/Q_j$

Lower energy dissipation rate induces narrower cocoon

$$Q_j = \pi r_j^2 u_j \left(\Gamma_j^2 \rho_j h_j - \Gamma_j \rho_j c^2\right)$$

Turbulence energy dissipation rate

$$\mathcal{L}_{\rm turb} \approx \varphi \frac{E_{\rm turb}}{\tau_{\rm cascade}},$$

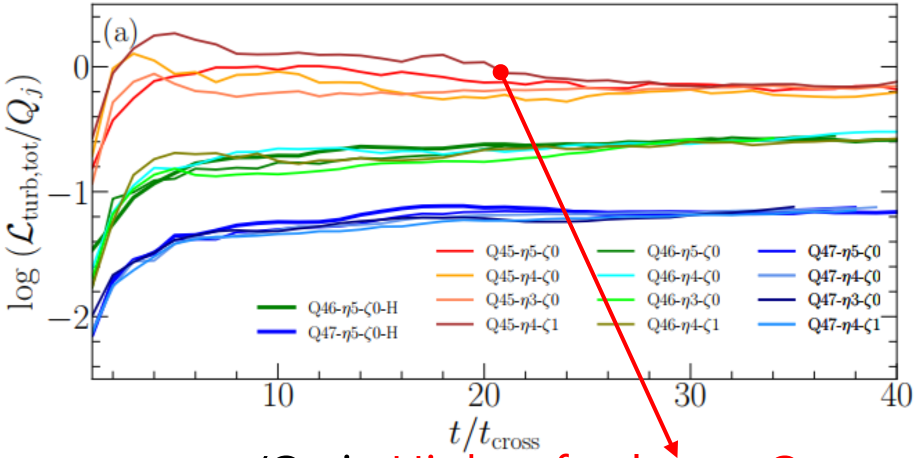

$\mathcal{L}_{\rm turb}/{\rm Q}_j$ is Higher for lower ${\rm Q}_j$

$\mathcal{L}_{\rm turb}/{\rm Q}_j$ is hardly depends on $\dot{M}$

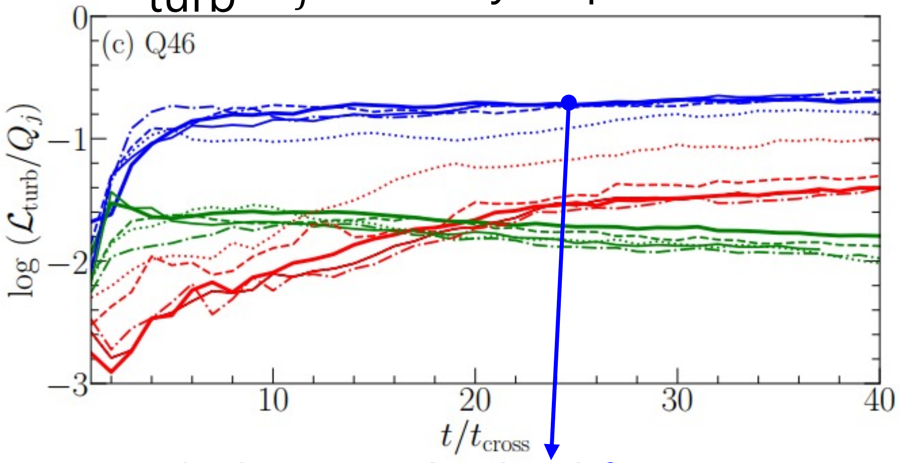

Turbulence in the backflow are most important in energy dissipation

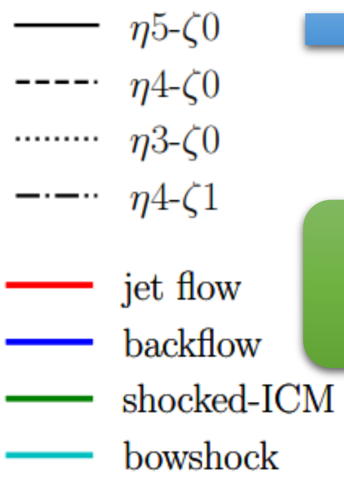

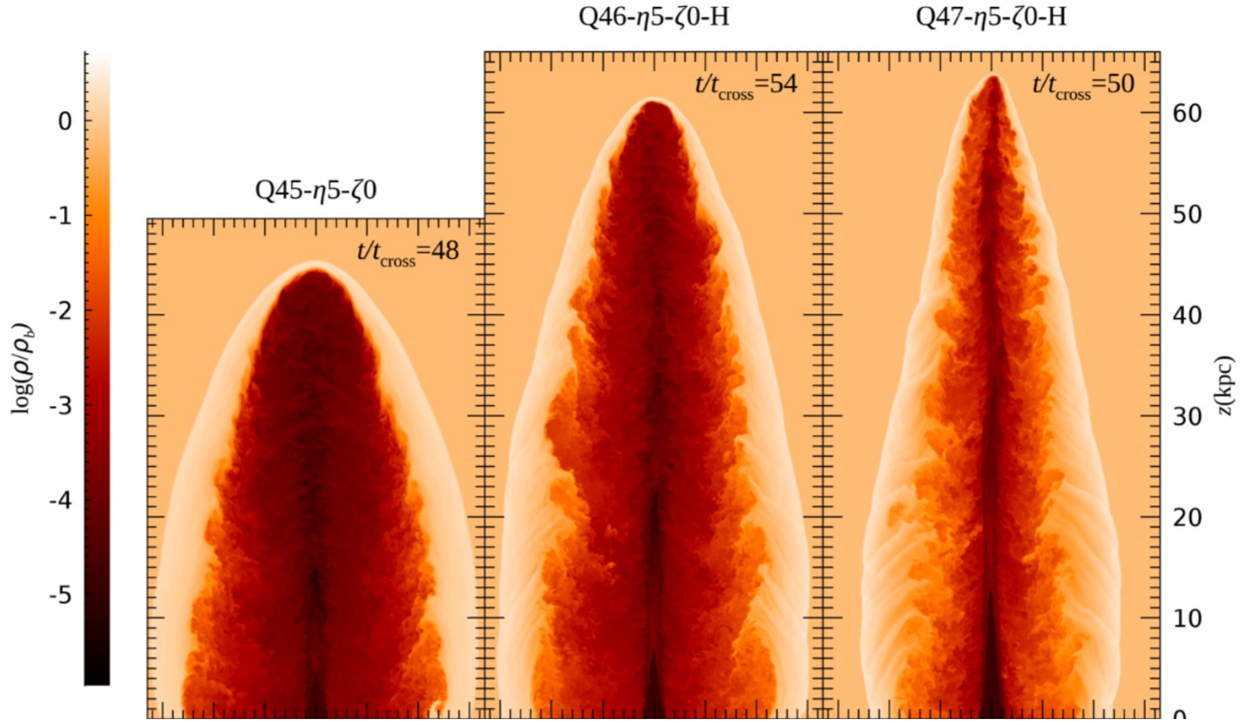

Higher Q_j, Lower $\mathcal{L}_{\rm turb}/{\rm Q}_j$

Lower energy dissipation rate induces narrower cocoon

$$Q_j = \pi r_j^2 u_j \left(\Gamma_j^2 \rho_j h_j - \Gamma_j \rho_j c^2\right)$$

Step 3. Monte Carlo Simulations for CR acceleration, using simulated FR-II jets

Three Main Particle Acceleration Mechanisms

Seo et al 2021

Diffusive Shock Acceleration

Shock Mach no.

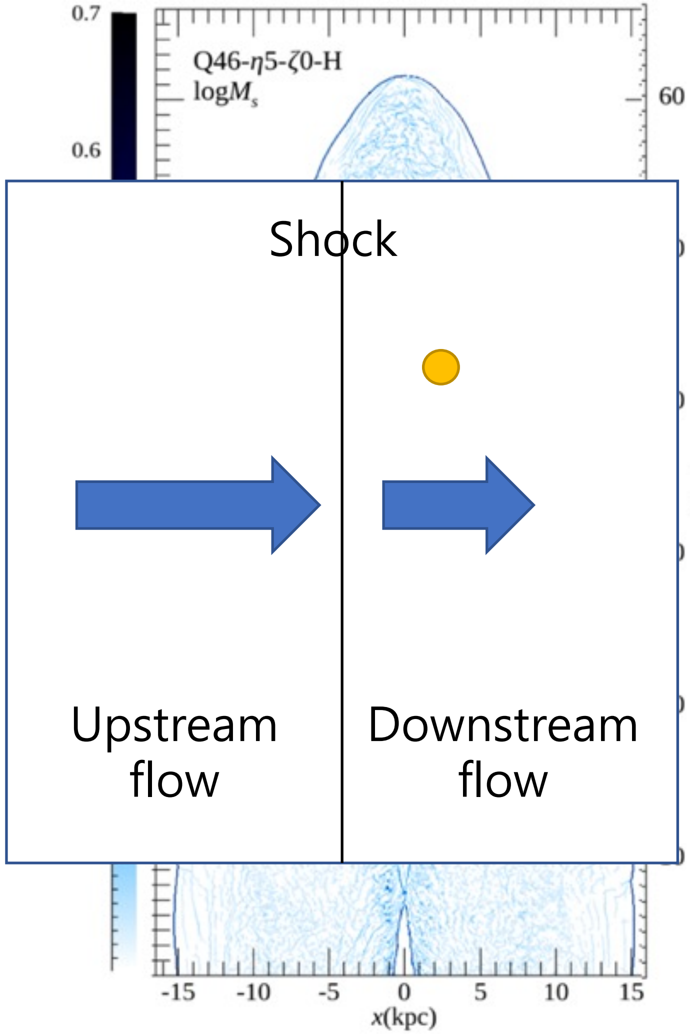

Shear Acceleration

Relativistic shear coefficient

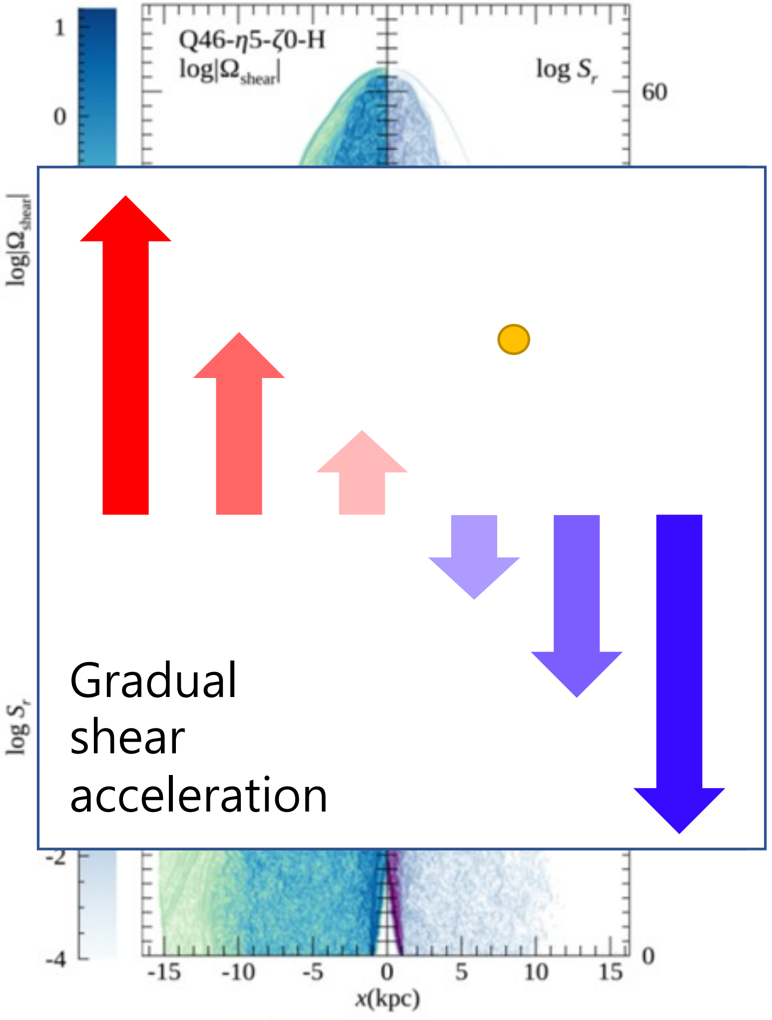

$$S_r = \frac{\Gamma_v^4}{15}\left(\frac{\partial v_z}{\partial r}\right)^2,$$

Turbulent Acceleration

Vorticity = turbulence

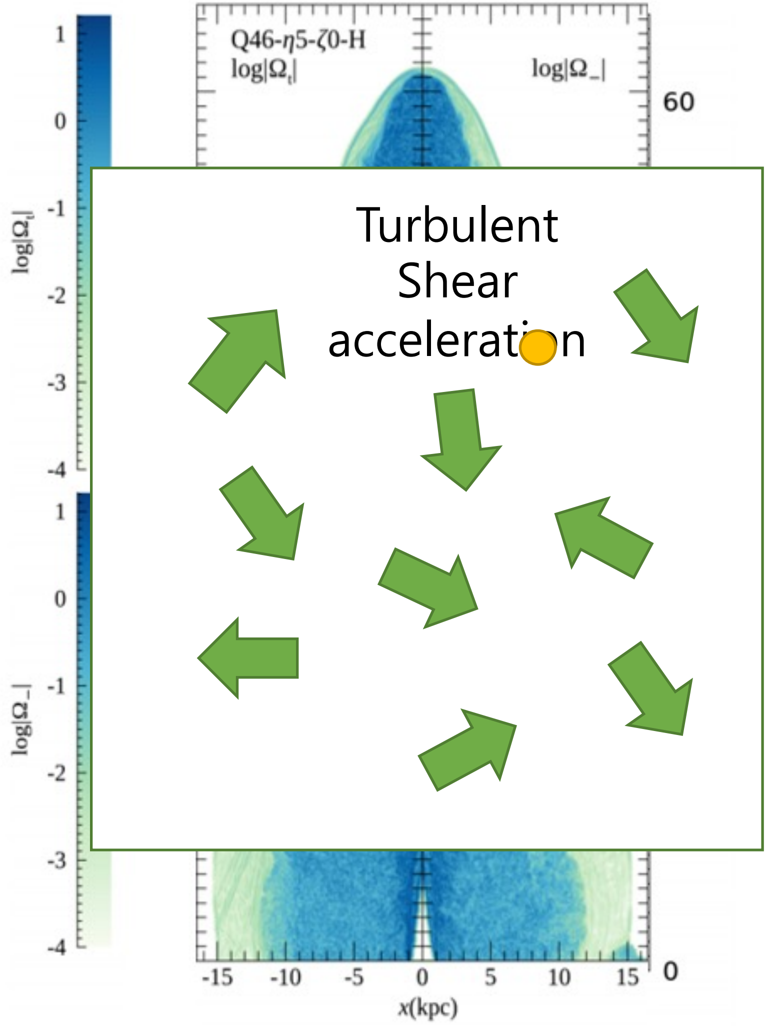

Cosmic ray transport (Monte-Carlo) Code test

Shock acceleration test

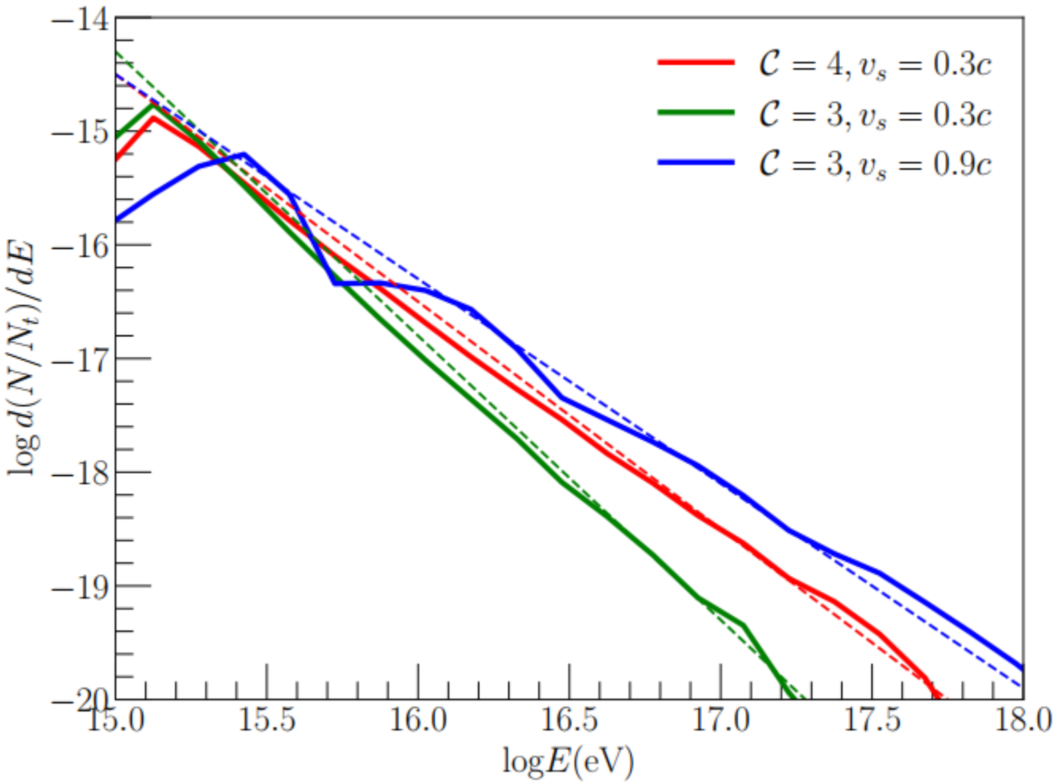

Shear acceleration test

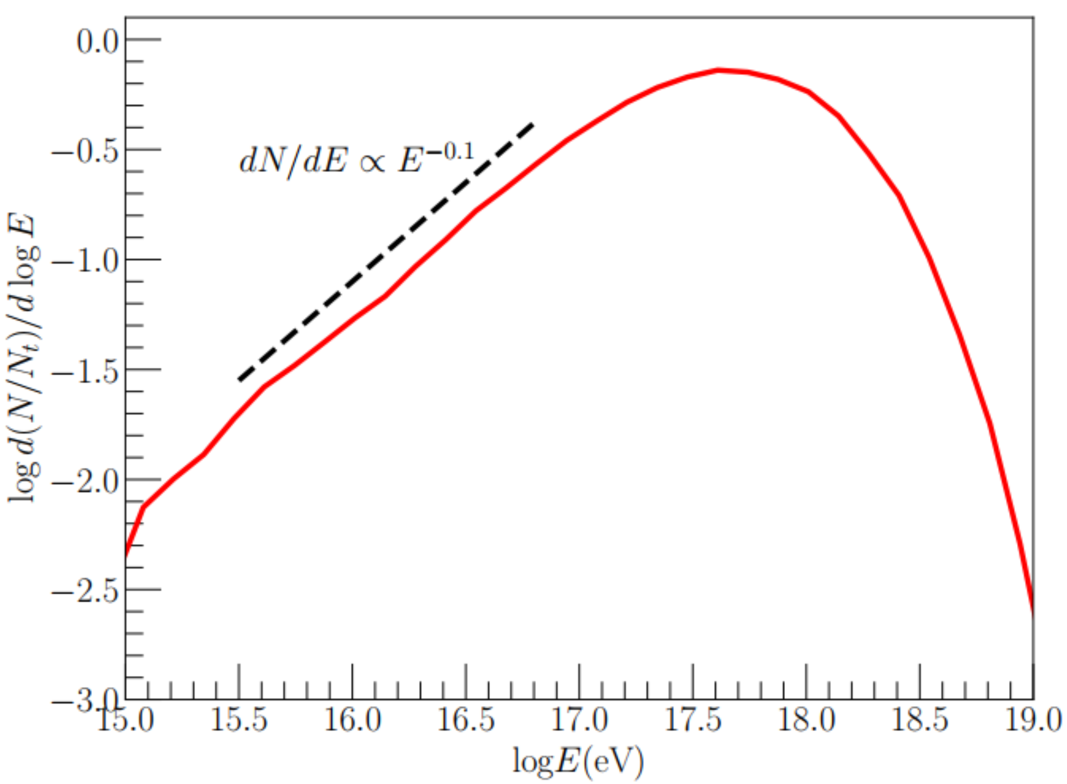

This method can reproduce an analytic solution of the stochastic acceleration processes.

Monte Carlo simulations for CR transport

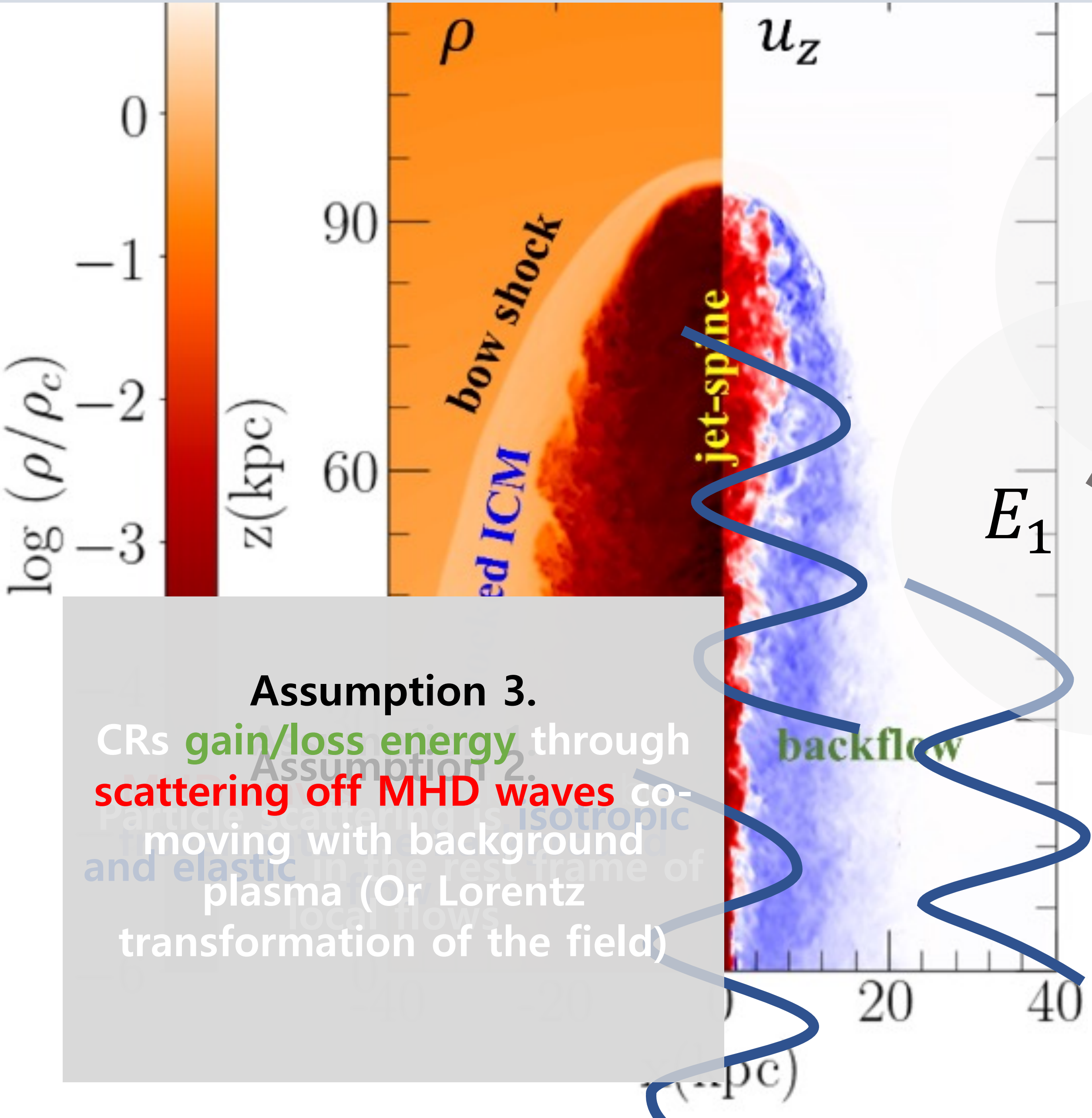

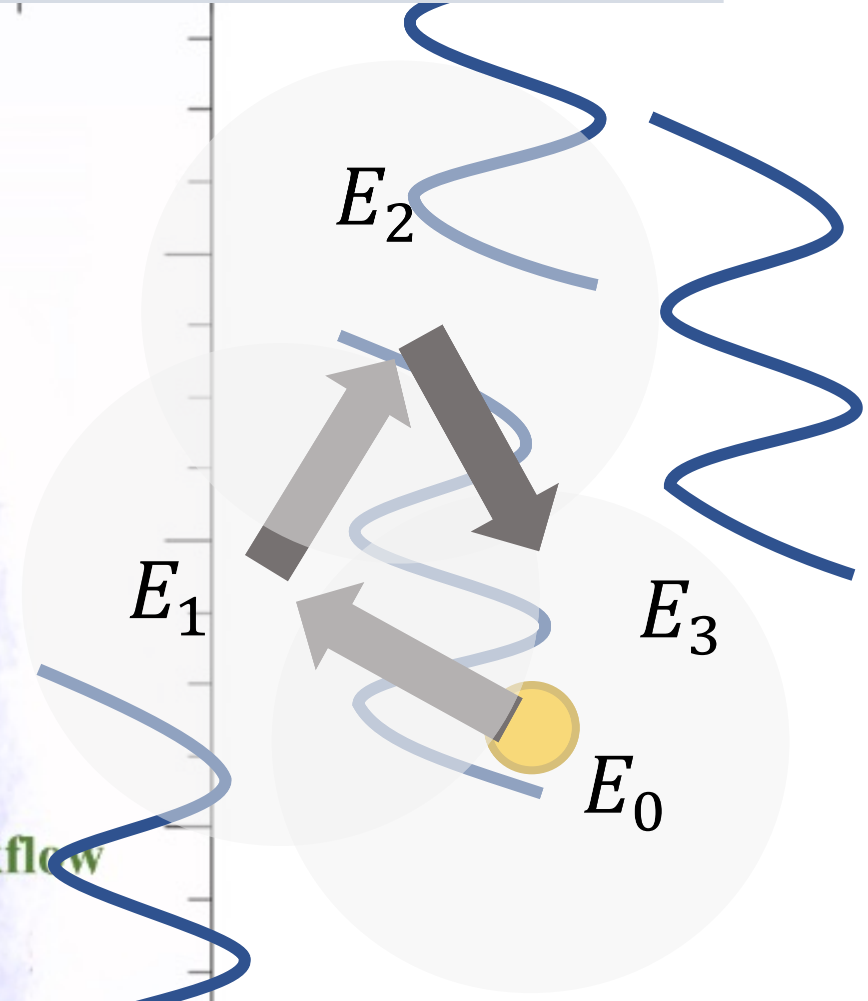

Assumption 3.

CRs gain/loss energy through scattering off MHD waves co-moving with background plasma (Or Lorentz transformation of the field)

Monte Carlo simulations for CR transport

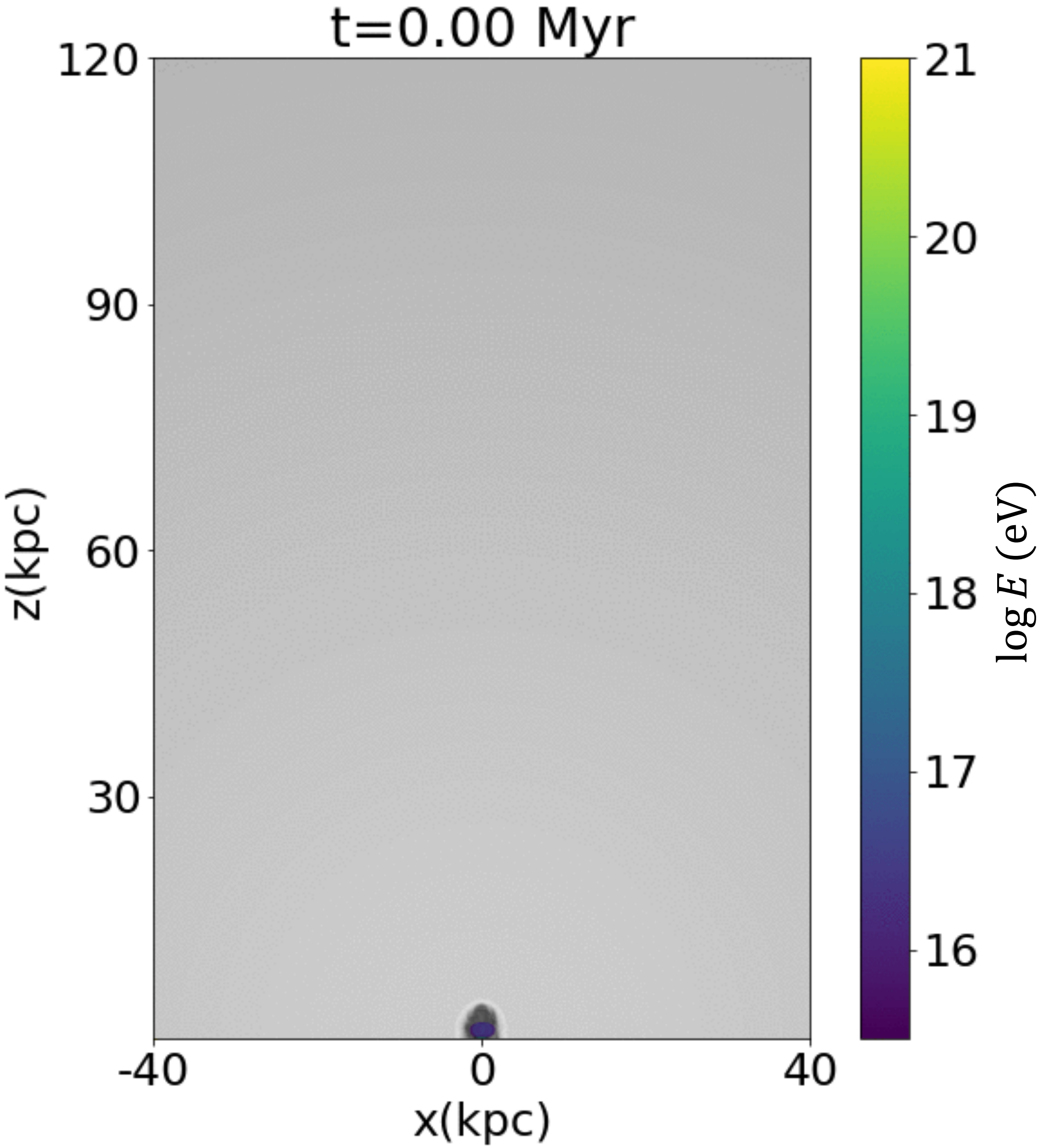

- **Initially CRs** : **10TeV-PeV($10^{13\text{-}15}$eV)** with power-law $dN/dE \propto E^{-2.7}$.
- CRs are **injected uniformly** at the jet nozzle.
- Particles are continuously injected and advected with evolving jet profile

Prescriptions for Particle Scattering

mean free path: $\lambda_{mf} \propto E^{\delta}$

$\boldsymbol{E < E_{coh}}$:

$$E_{\rm coh} = eZ_iBL_0 = 0.89 \text{ EeV} \cdot Z_i(B/1\mu\text{G})(L_0/1\text{kpc})$$

Kolmogorov scattering

Scattered with **MHD waves (with Kolmogorov spectrum)**

➔ $\lambda_{mf} \propto E^{\frac{1}{3}}$

Bohm scattering only at shocks

scattered with **self-generated waves near shocks**.

➔ $\lambda_{mf} \propto E$

$\boldsymbol{E > E_{coh}}$: **Non-resonant scattering**

Mean free path is **larger** than **the scale of turbulence**.

➔ $\lambda_{mf} \propto E^2$

Prescriptions for magnetic field

- **Internal energy model**

$$\frac{B_p^2}{8\pi} = \frac{p}{\beta}.$$

- **Turbulence kinetic energy model**

$$\frac{B_{turb}^2}{8\pi} \approx KE_{turb}$$

- **Shock amplification model**

$$\frac{B_{Bell}^2}{8\pi} \approx \frac{3}{2}\frac{v_s}{c}P_{CR} \approx \frac{3}{2}\frac{v_s}{c}(0.1\rho_1 v_s^2)$$

$$\Rightarrow \quad B_{\mathrm{comov}} = \max(B_p, B_{\mathrm{turb}}, B_{\mathrm{Bell}})$$

$B_{\mathrm{obs}} \approx \Gamma B_{\mathrm{comov}}$ in the simulation frame

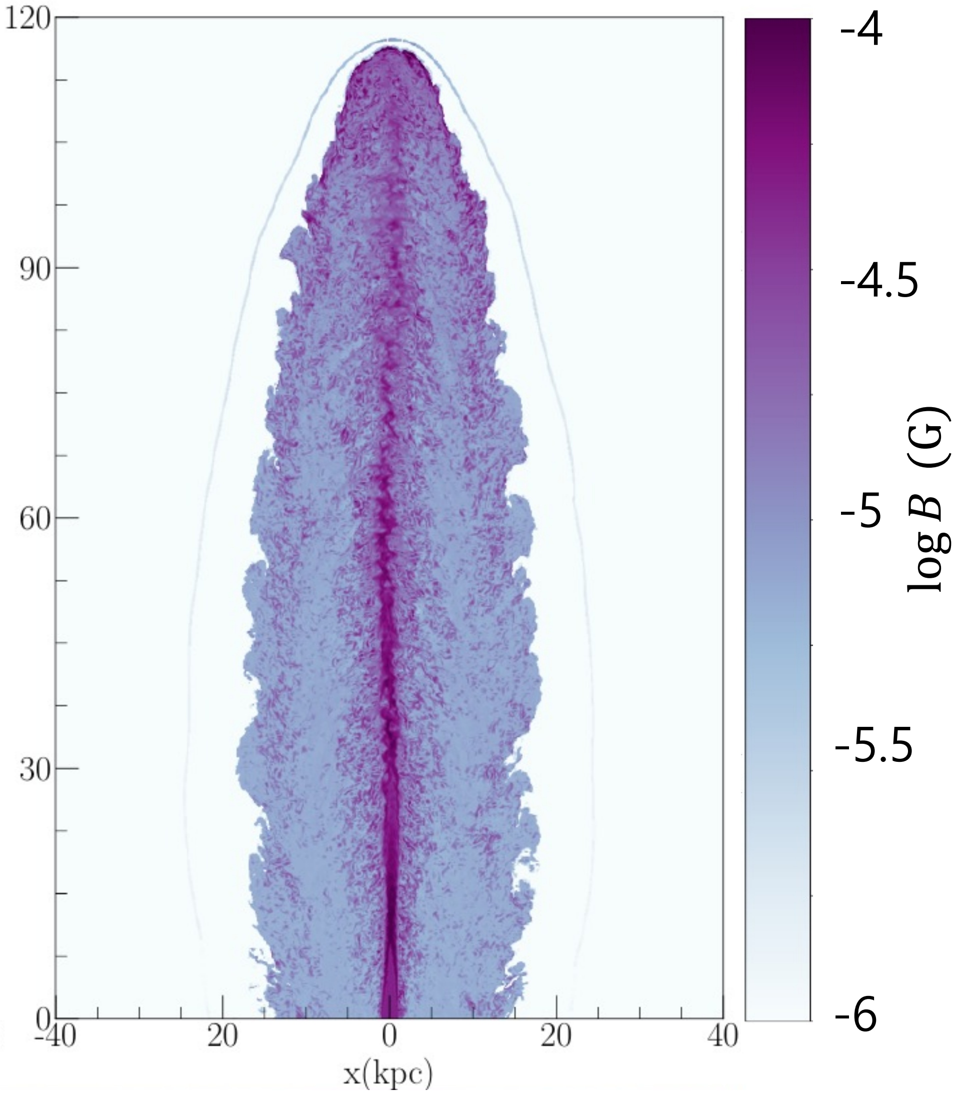

in the simulation frame

Jet: B ~ $100\mu G$
Backflow: B ~$10\mu G$
ICM: B ~$1\mu G$

Acceleration Time scales

This simulation only follows energy changing with scattering.
Q : How do we determine the primary acceleration process in each scattering?

A : Among the **three different acceleration processes**,
the acceleration process with the **shortest t_{acc}** would be the most dominant one.
➔ selected as the **primary acceleration process.**

DSA (shock)

$$t_{\mathrm{DSA}} = 3.52\times10^{3}\mathrm{yr}\frac{\chi(\chi+1)}{\chi-1}\left(\frac{v_s}{c}\right)^{-2}\left(\frac{E}{\mathrm{EeV}}\right)\left(\frac{B}{1\mu\mathrm{G}}\right)^{-1}$$

Drury 1983

Gradual Shear Acc

$$t_{\mathrm{GSA}} = 4.90\times10^{4}\mathrm{yr}\frac{1}{(4+\alpha)\gamma^4}\left(\frac{\Omega_{shear}}{c/r_j}\right)^{-2}\left(\frac{\lambda_f(p)}{\mathrm{kpc}}\right)^{-1}$$

Webb et al 2018

Turbulent Shear Acc

$$t_{\mathrm{TSA}} = 2.88\times10^{4}\mathrm{yr}\left(\frac{L_0/\gamma}{1\mathrm{kpc}}\right)^{\frac{2}{3}}\left(\frac{|v_{tur}|}{c}\right)^{-2}\left(\frac{\lambda_f(p)}{\mathrm{kpc}}\right)^{1/3}$$

Ohira 2013

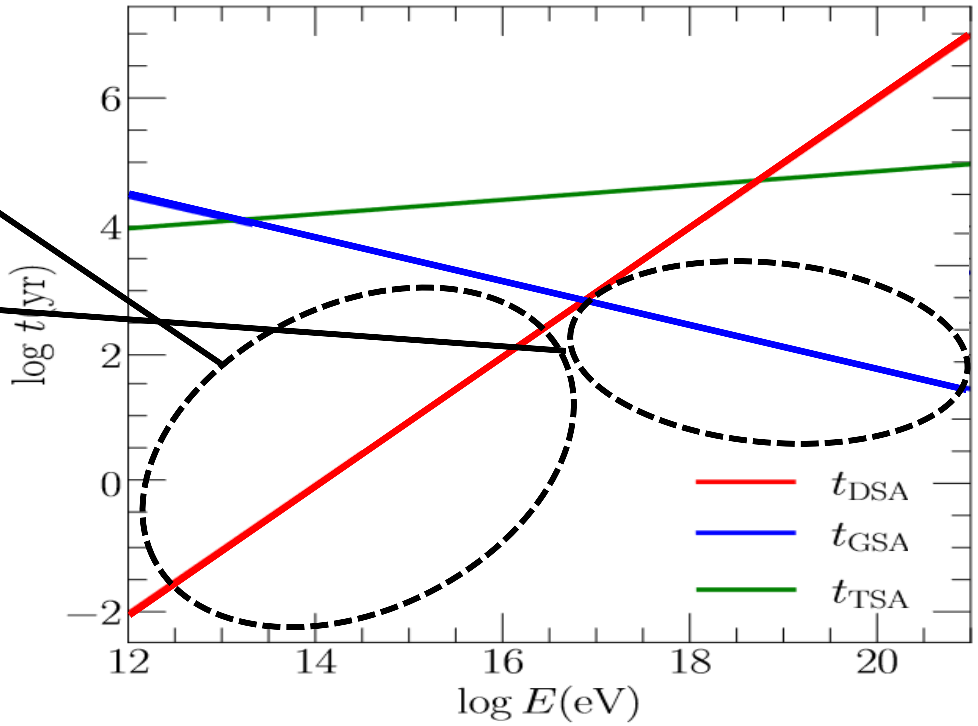

Acceleration time scales for different processes in common jet region

Sample trajectory

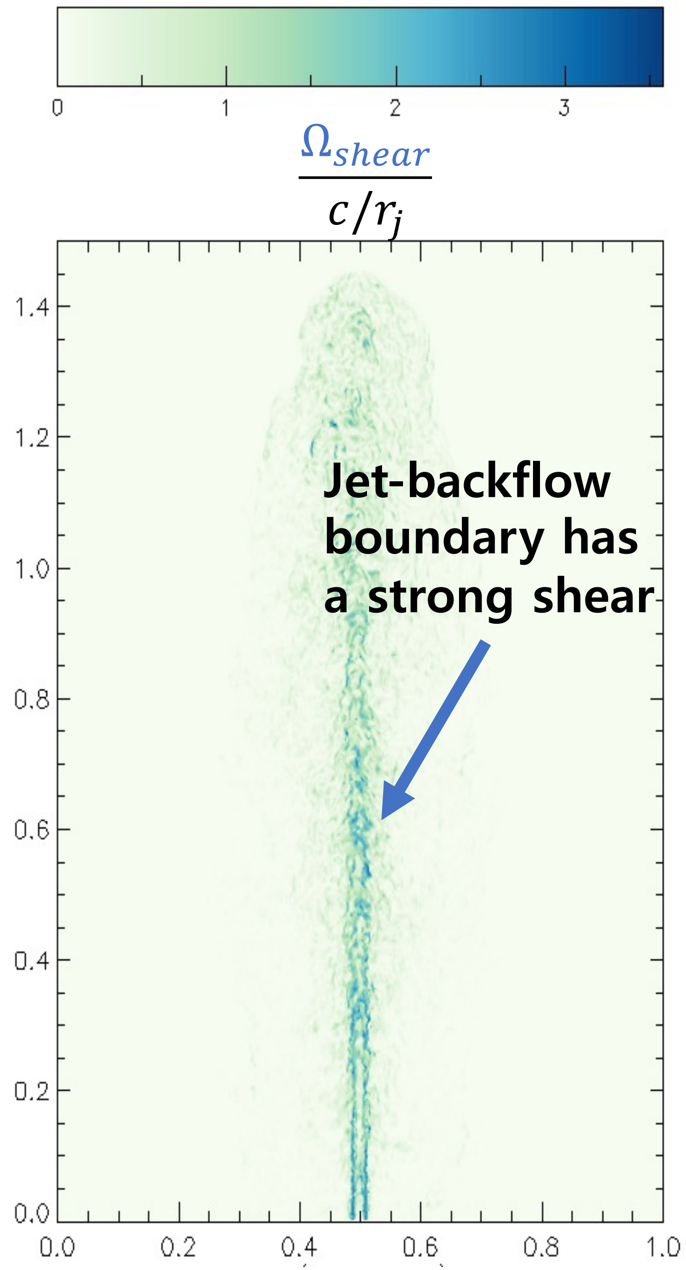

Jet-backflow boundary has a strong shear

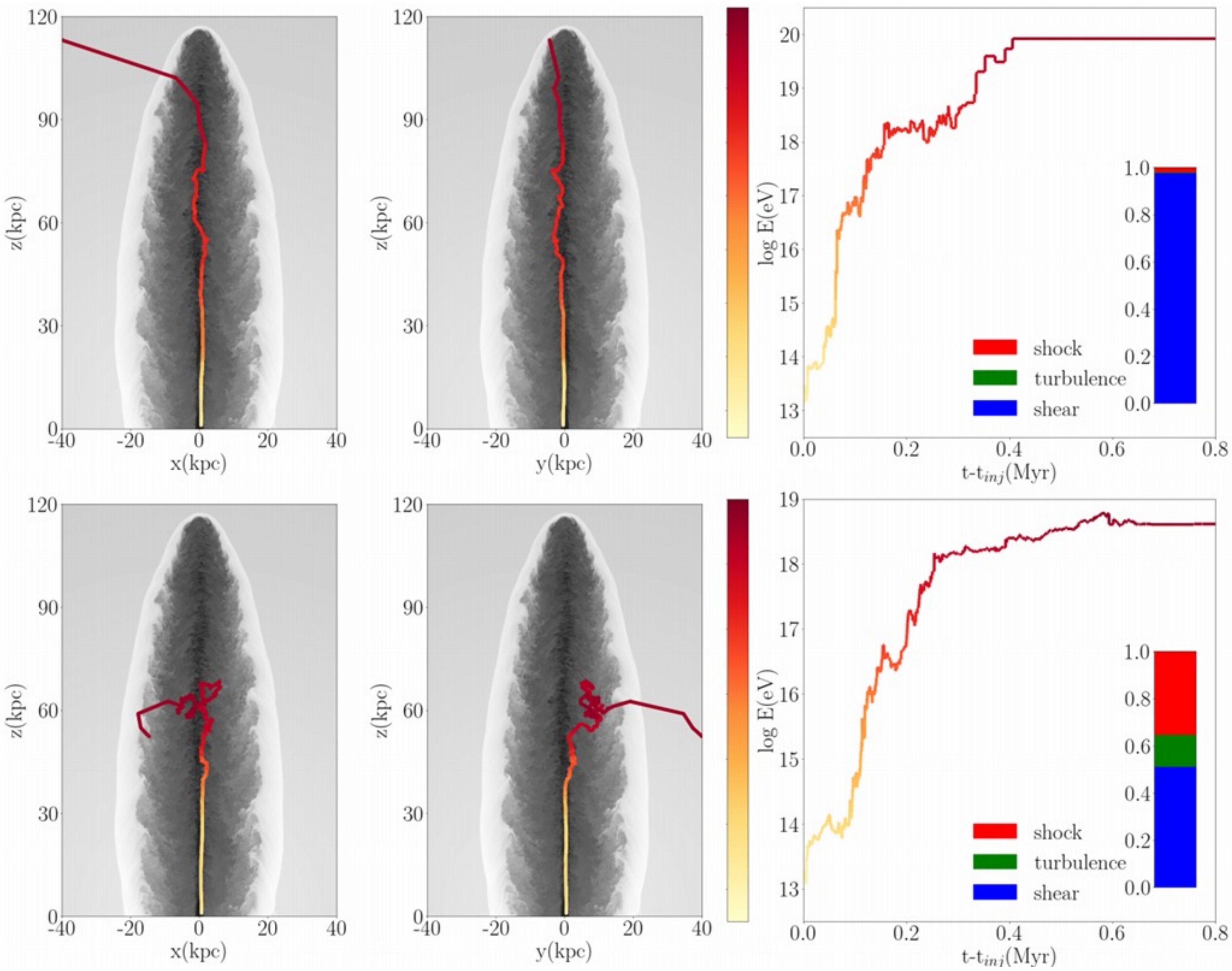

Particle energy spectrum

- Accelerated particles has a **power-law** spectrum with a cutoff.
- The slope of the power-law is $\boldsymbol{\frac{dN}{dE}} \propto \boldsymbol{E^{-0.4} - E^{-0.8}}$, depending on the scattering law.
- In **early time**, maximum energy is determined by the **age of the jet**, while in the **late stage**, it is controlled by the **cocoon width**.

age-limited

$$E_{\rm max,a} \approx \left[\frac{(t_{\rm age}c)\Gamma_z^2\beta_z^2}{\zeta L_0}\right]^{1/2} E_{\rm coh}.$$

size-limited

$$E_{\rm max,s} \approx E_{\rm coh}\left[\mathcal{W}\frac{r_j}{L_0}\right]^{1/2} \approx 4\,{\rm EeV}\cdot Z_i(\frac{B}{1\mu{\rm G}})(\frac{L_0}{1{\rm kpc}})(\frac{\mathcal{W}}{20})^{1/2}.$$

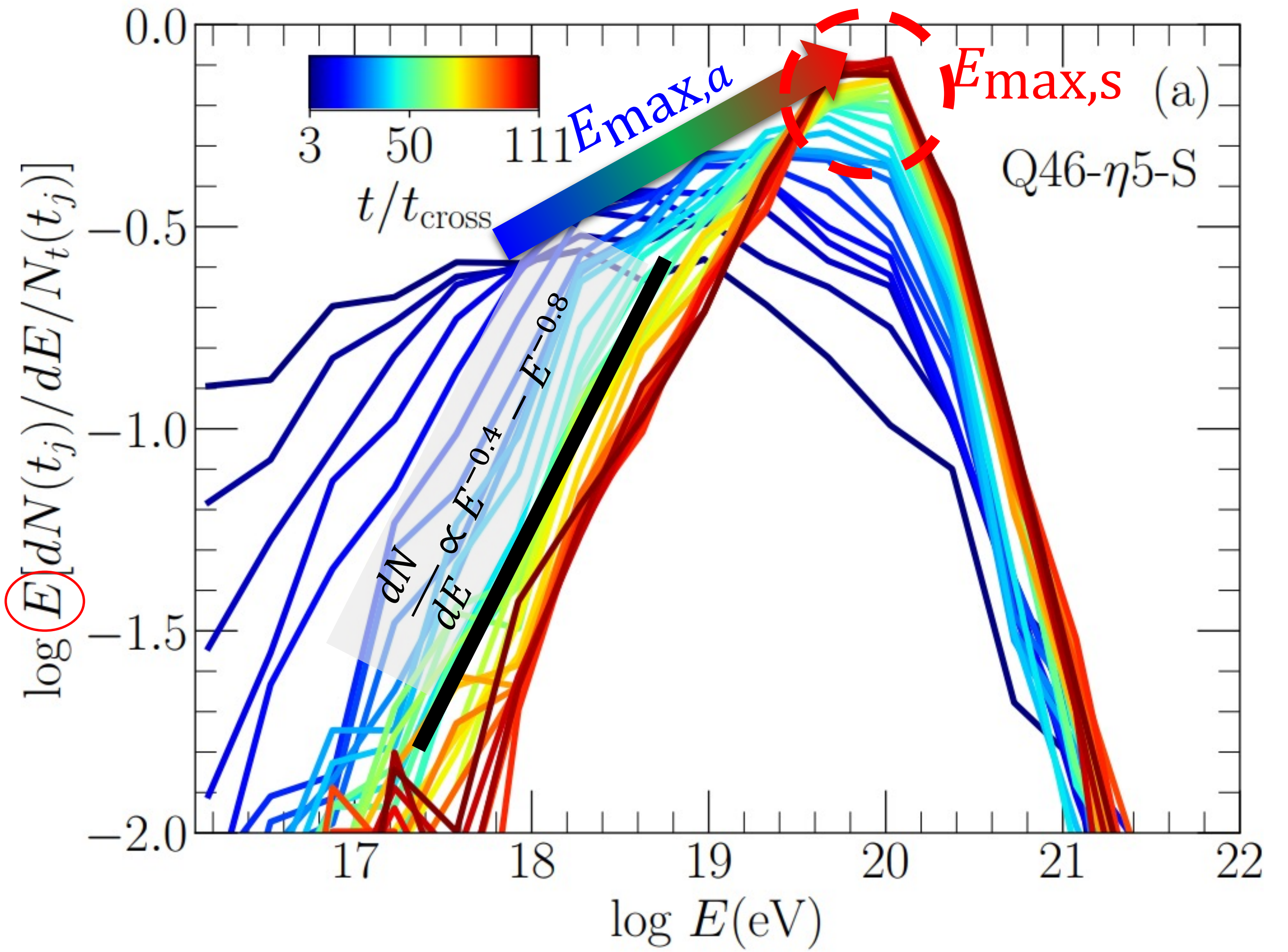

Evolution of the energy spectrum of escaping particles, line color indicates **time**.

Distribution of energy gains for accelerated particles

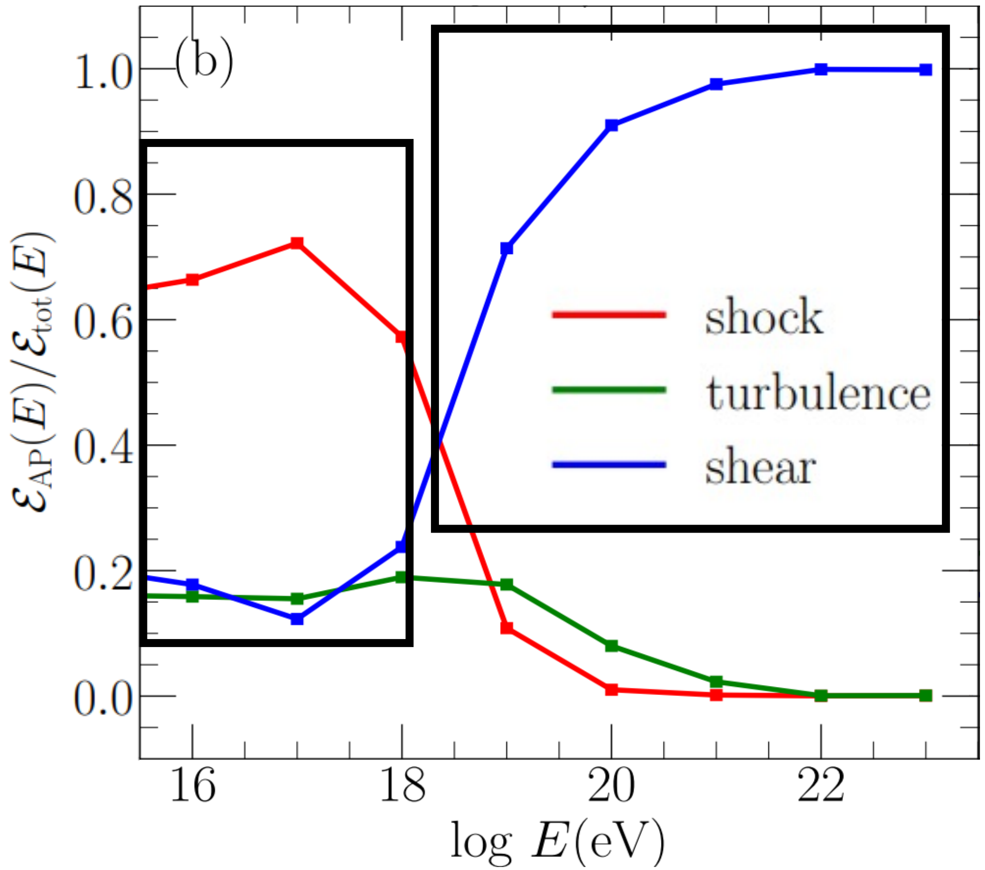

$\varepsilon_{AP}(E)/\ \varepsilon_{tot}(E)$

Model name	$\frac{\tilde{\mathcal{E}}_{\rm shock}}{\tilde{\mathcal{E}}_{\rm tot}}$ (%)	$\frac{\tilde{\mathcal{E}}_{\rm turb}}{\tilde{\mathcal{E}}_{\rm tot}}$ (%)	$\frac{\tilde{\mathcal{E}}_{\rm shear}}{\tilde{\mathcal{E}}_{\rm tot}}$ (%)
High power FRII	1.4	6.1	92.5

fractions of the cumulative energy gain due to different Acceleration Process:
where AP = shock, turbulence, & shear

Here, $\varepsilon_{AP}(E)$ is the sum of ΔE of all scattering events tagged as a given type of AP for the particles whose final energy E lies in the logarithmic bin of [log E, log E + d log E]

For high-energy particles, the energy gain by **shear acceleration** is dominant.
Shear acceleration is the primary mechanism to generate **UHECRs.**
Shock acceleration contributes to the production of UHECRs up to Hillas energy of the shock.
Turbulence acceleration plays a secondary role.

Restricted random walk model

In a realist jet flow, there may **not** be **magnetic fluctuations strong enough** to scatter in a random walk manner for **high energy particles**

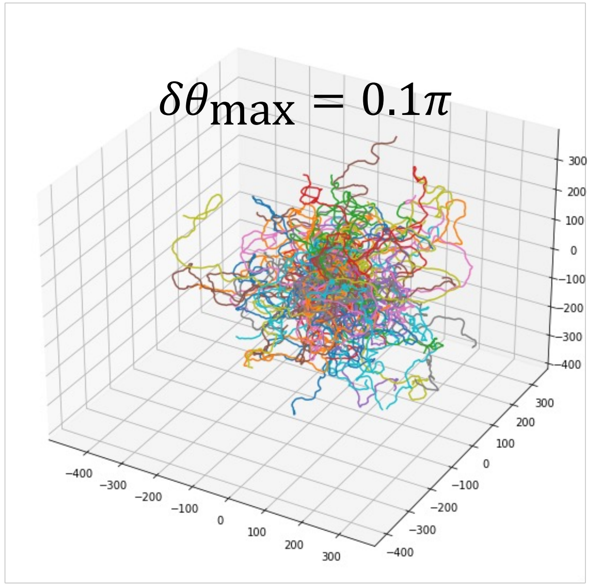

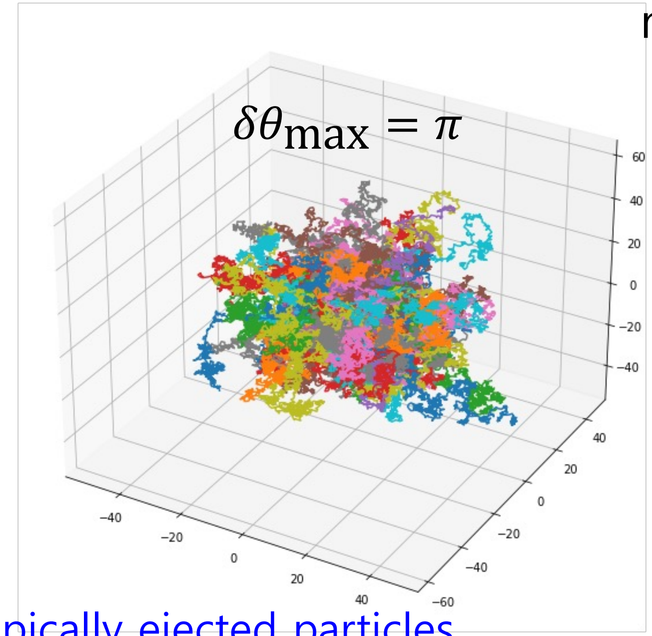

Sample trajectory of the isotopically ejected particles with restricted random walk model

$$\delta\theta_{max} = \pi \min[1, \psi \frac{L_0}{\lambda_f}] \qquad \begin{array}{cc} \lambda_f(E) \gg L_0 & \lambda_f(E) \ll L_0 \\ \delta\theta_{\max} \ll 1. & \delta\theta_{\max} \approx \pi. \end{array}$$

With higher restriction, acceleration of the high energy particles less effectively occurs.

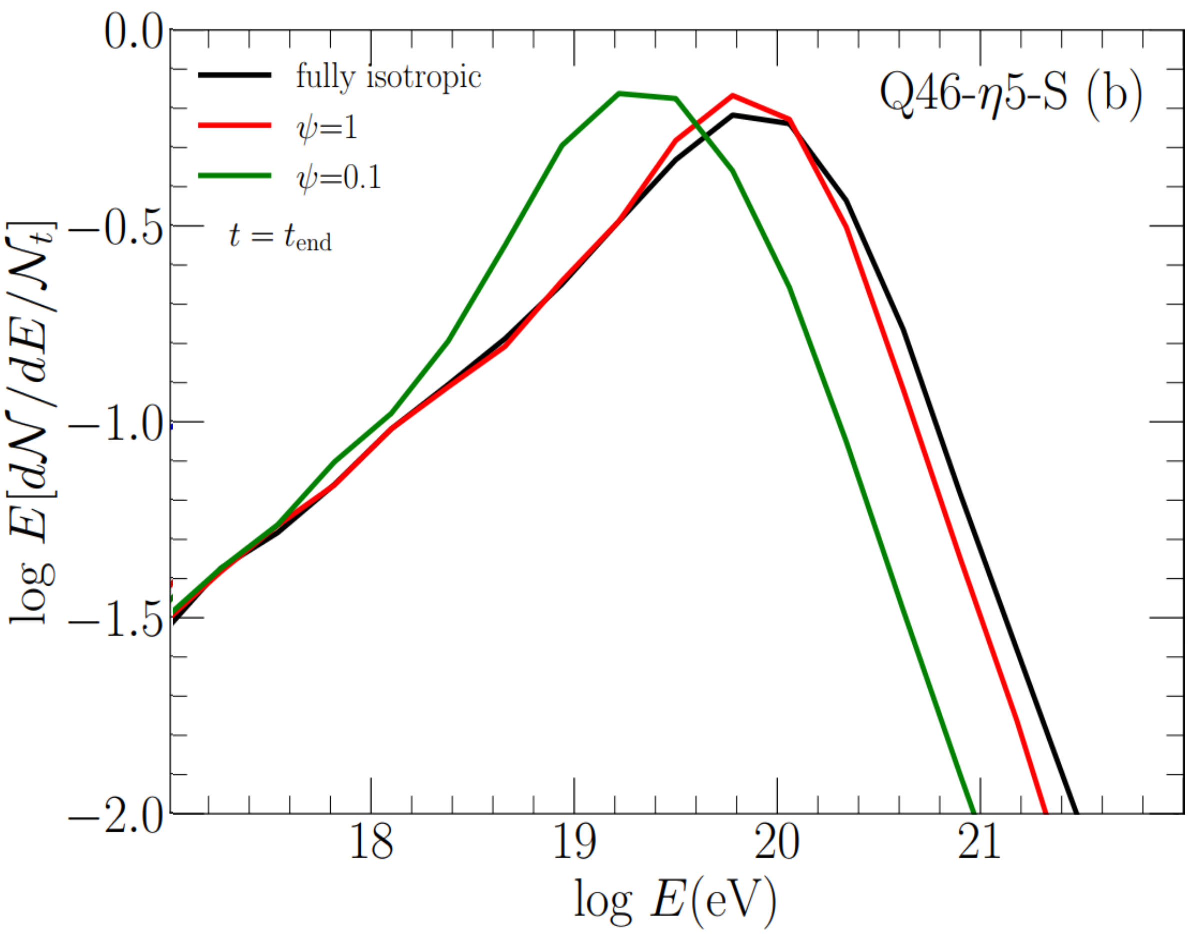

Energy spectrum of the escaping particles which have different ψ

Jet power dependency

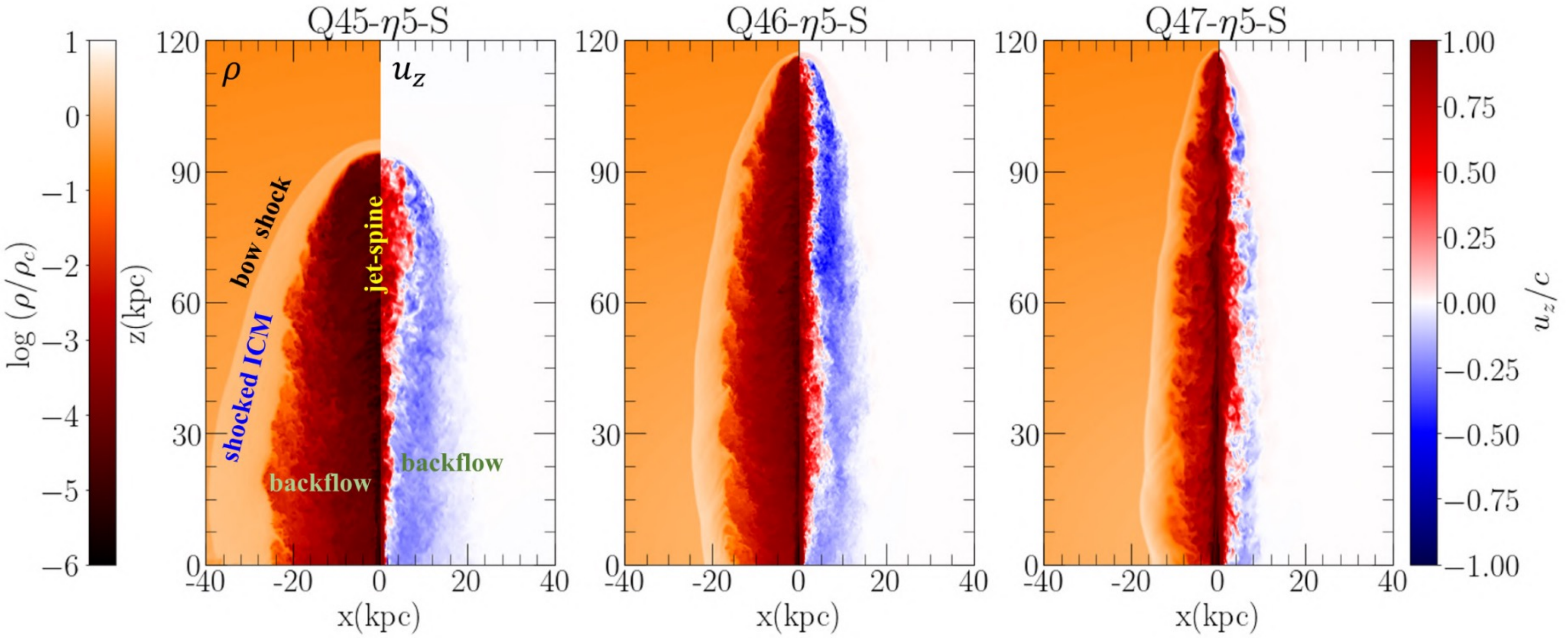

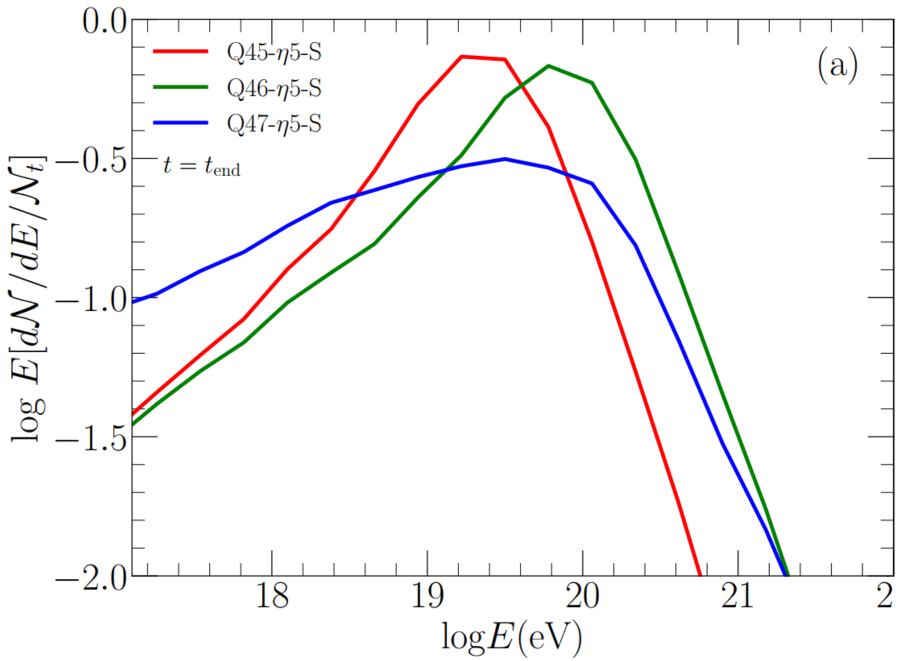

- **Slope**
  Power-law slope is **harder** when the **jet power** is **lower**, due to the amount of the non-linear structures (more efficient DSA and TSA) contained in a cocoon.

- $\boldsymbol{E_{cut}}$
  Depending on the **cocoon width** and **strength of the magnetic field**. Higher jet power cases have higher E_{cut}, because of the strong magnetic field. Q47 model has extremely thin cocoon, hence it prevents further nGSA.

Mean free path model dependency

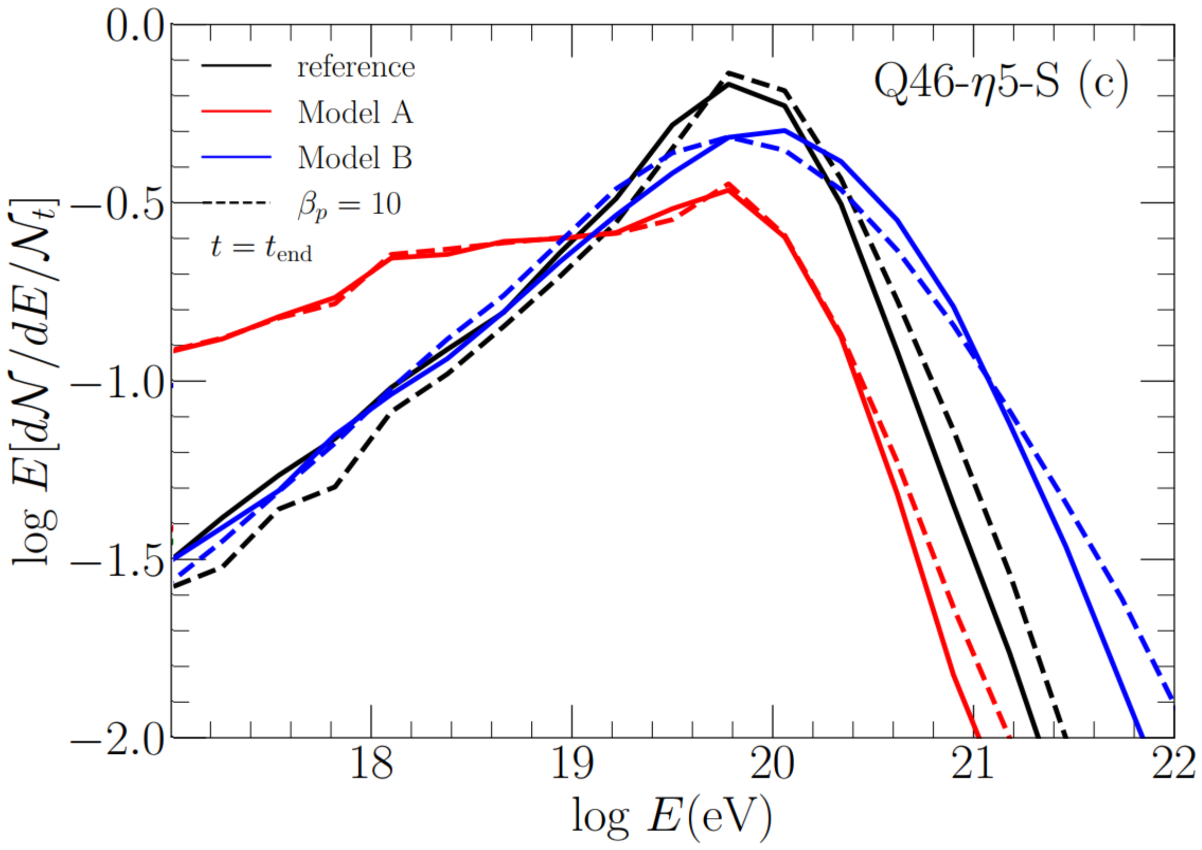

mean free path:	$\lambda_f = (E/E_{\rm coh})^{\delta} L_0,\ E_{\rm coh} = eZ_iBL_0$
reference:	$E < E_{\rm coh}$: $\delta = 1/3$, $\delta = 1$ (at shocks)
	$E > E_{\rm coh}$: $\delta = 2$
model A:	$E < E_{\rm coh}$: $\delta = 1/3$
	$E > E_{\rm coh}$: $\delta = 2$
model B:	$E < E_{\rm coh}$: $\delta = 1/3$, $\delta = 1$ (at shocks)
	$E > E_{\rm coh}$: $\delta = 1/3$
Kolmogorov scattering:	$\delta = 1/3$
nonresonant scattering:	$\delta = 2$
Bohm scattering:	$\delta = 1$

Model A: for $E_{coh} > E$, $\lambda_{Kolmo} > \lambda_{Bohm}$, less acceleration can occur
Model B: for $E_{coh} < E$, $\lambda_{Kolmo} < \lambda_{non-res}$, Further acceleration can occur
Low beta (stronger B field) : smaller mean free path induces further acceleration

Summary

New features in our RHD code

1. 5^{th} order accurate **WENO** scheme **(Jiang & Shu 1996, Jiang & Wu 1999)** for spatial integration
2. strong stability preserving Runge-Kutta (**SSPRK**) scheme **(Spiteri & Ruuth 2002)** for time integration
3. Realistic equation of state (**RC**, Ryu et al 2006) to treat the flow with γ=4/3- 5/3
4. Transverse-flux averaging for multi-dimensional flows **(Buchmüller et al. 2016)**
5. Modification of eigenvalues for Suppression of Carbuncle Instability **(Fleischmann et al. 2020)**

Application:

1. **Relativistic jets:** we can identify and analyze non-linear structures such as shocks, shear, & turbulence.
2. Using **Monte Carlo simulations** for CR transport through the simulated jet flows, we can study the acceleration of Ultra-high energy cosmic rays through shocks, shear & turbulence.